Malaysian Journal of Catalysis
http://mjcat.utm.my/
MJCat Research Article

Hydrogenation of Glucose into Sorbitol using Ru-based Catalyst: A Short Review

Z.A. Alexzman [a], N.H.R. Annuar [a,*]

[a]*Faculty of Applied Sciences, Universiti Teknologi MARA, Cawangan Johor, Kampus Pasir Gudang, 81750 Masai, Johor, Malaysia.*

**Corresponding Author: nurha8558@uitm.edu.my*

Article history :
Received 29 Jun 2021
Accepted 30 September 2021

GRAPHICAL ABSTRACT

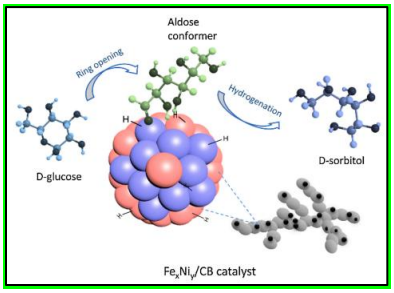

ABSTRACT

Glucose is one of the most abundant non-food biomasses on the earth, and it is one of the most promising fossil-fuel alternatives for the long-term production of commodity chemicals and fuels, with the potential for carbon-neutral technologies. Sorbitol produced by glucose hydrogenation, is the most potential carbohydrate-derived building block chemicals has been regarded as a promising alternative to petroleum and natural gas in future refinery. Catalytic hydrogenation of glucose into sorbitol has recently drawn attention. Heterogenous catalysts are preferred in this reaction due to their high efficiency and reusability. This paper discusses the catalytic performance and reusability of Ru-based catalysts, which has been demonstrated in numerous studies to have a high selectivity toward target products. The reaction mechanism of the glucose hydrogenation over a few heterogenous catalyst are also being highlighted. Additionally, critical challenges and potential future research approaches for heterogeneous catalytic hydrogenation of glucose to sorbitol are highlighted.

Keywords: Biomass; sorbitol; glucose hydrogenation; Ru-based catalyst

| eISSN 0128-2581 |

1. INTRODUCTION

The Twelfth Malaysia Plan (12MP) for the period 2021-2025 is consistent with the shared prosperity initiative, which encompasses three dimensions; economic empowerment, environmental sustainability, and social re-engineering. It incorporates the blue economy, green technology, renewable energy, as well as climate change adaptation and mitigation [1]. The utilization of lignocellulosic biomass as a renewable raw material for both energy and valuable platform chemicals can be related to the 12MP dimension as biomass is listed in five types of renewable energy.

Due to the depletion of fossil energy resources and pressing environmental concerns, cellulosic biomass appears to be one of the most promising alternatives for producing chemicals, energy, and fuels [2]. Lignocellulose is the most abundant non-edible biomass source found in plant walls. It is composed of carbohydrate polymers cellulose and hemicellulose that are embedded in a lignin matrix. Unlike fossil fuels such as petroleum or coal, cellulose, as well as a primary source of monosaccharides, including glucose and fructose, has a high content of oxygen in its structure (c.a. 50 wt.%) in addition to hydrogen and carbon elements, which is a significant advantage in the synthesis of oxygen-containing chemicals such as sugar alcohols [3-4]. Cellulose is a promising raw material that is easier to distinguish than hemicellulose and lignin, and it can be employed in the conversion of various platform chemicals in the presence of various catalysts.

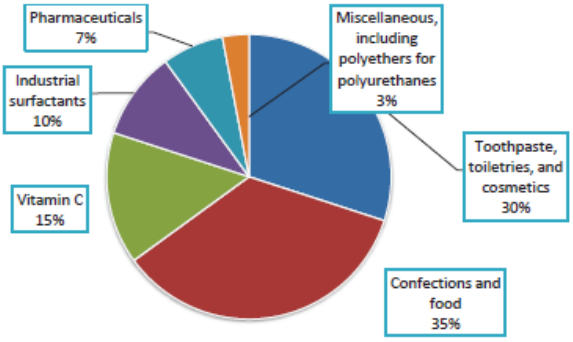

Figure 1: Major application of sorbitol [6].

According to US Department of Energy, sorbitol is one of the top 12 bioderived building blocks that can be easily converted into fuels and chemicals [5]. It is primarily employed in food and beverage, pharmacy, and cosmetic items, as well as an intermediate product in the manufacture of vitamin C, as seen in Figure 1 [6]. On a small scale, sorbitol can be extracted from various fruits such as apples, pears, peaches, apricots, and nectarines, and also dried fruits and some vegetables [7], but the most common reaction route for its industrial production is glucose hydrogenation.

Almost all sorbitol synthesis processes currently in use are based on the hydrogenation of glucose catalysed by metallic catalysts. High efficiency, ease of use, cheap cost, and relative environmental safety make the catalytic technique of sorbitol manufacturing employing heterogeneous systems increasingly viable [8]. Catalyst development in terms of controlled particle formation and modification of porosity, acidity, basicity, and metal support interactions resulted in an increase in catalytic performance [9]. Based on previous literature, Ru-based catalyst gave the highest activity and selectivity toward glucose reduction [10]. To our knowledge, however, the review on the influence of Ru-based catalysts in glucose hydrogenation, particularly in the manufacture of sorbitol, remains inadequate. Recent research and the performance of glucose hydrogenation over Ru-based catalysts, as well as the reaction mechanism over heterogenous catalysts that produces the required products, are discussed in this review.

2. HYDROGENATION OF GLUCOSE

Glucose, also known as dextrose, is a type of carbohydrate known as a simple sugar (monosaccharides). C6H12O6 is the chemical formula for glucose and it can be found in fruits and honey, and it's the most common free sugar in higher animals' blood. Andreas Marggraf isolated glucose from raisins for the first time in 1747. Jean Dumas invented the name glucose in 1838, derived from the Greek word gleucos, which means "sweet" or "sugar," while Emil Fischer found the structure around the turn of the century [11]. Glucose is the most abundant form of simple sugars, and it can be acquired via acidic or enzymatic hydrolysis of large natural polysaccharides like cellulose and starch [12]. D-(+)-glucose is a 2,3,4,5,6-pentahydroxyhexaldehyde with a molecular weight of 180.16 kDa. D-Glucose is a polyalcohol as well as an aldehyde. It is classified as an aldose, which is a sugar with an aldehyde group. The suffix -ose denotes a sugar group, while -ald denotes an aldehyde group, which is responsible for the majority of chemical reactions of glucose [10]. Some of the physical properties of glucose are listed in Table 1.

All carbohydrate molecules contain hydroxyl groups which are available for reaction. Glucose and most other molecules of low molecular weight carbohydrates also have carbonyl groups available for the reaction. Hydrogenation is a chemical reaction in which hydrogen is added to a double bond formed between the oxygen atom and the carbon atom in the carbonyl group of an aldose or ketose contained in carbohydrates. D-glucose can be easily hydrogenated with hydrogen gas under pressure in the presence of catalyst. The product is d-glucitol, which is frequently referred to as sorbitol, with the suffix -itol denoting a sugar alcohol (an alditol) [11].

Table 1: Physical properties of glucose [8].

Physical Properties	Characteristics
Appearance	White, crystalline
Molecular weight	180.16 gmol-1
Melting point	150 C
Density	1.5620 g cm-3 (at 18 C)
Solubility in:	
Water	Very soluble
Ethanol	Slightly soluble
Ethyl Ether	Insoluble
Pyrimidine	Soluble

Sorbitol is produced by the hydrogenation of D-Glucose solutions obtained by hydrolysis of starch-containing crops (D-Glucose concentration up to 65 wt. %) in discontinuous batch slurry reactors at hydrogen pressures ranging from 5 – 15 MPa and temperatures between 100 and 180 ºC. Some by-products can be obtained during the hydrogenation process as a result of various side reactions as shown in Scheme 1: 1) D-Glucose can isomerize into fructose and mannose by Lobry de Bruyn–Alberda van Ekenstein rearrangements [13], which are further hydrogenated into mannitol and sorbitol [14], 2) The obtained sorbitol from the hydrogenation of D-Glucose, can be also isomerized into mannitol [15].

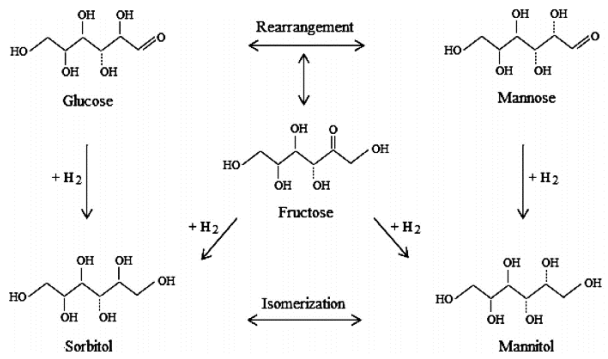

Scheme 1: Reaction network for glucose hydrogenation [10]

In order to obtain high reaction rate and products selectivity, a homogenous or heterogenous catalyst is often used [16]. Generally, homogeneous catalysts are present in the same phase as the reactants used in a chemical reaction, whereas heterogeneous catalysts are present in a different

phase than the reactants, i.e., the catalysis is typically in a solid phase while the reactant is in a gaseous or liquid state [17]. Dissolvable homogeneous catalysts always record high catalytic activity because of the numerous catalytic sites available [18]. However, the difficult separation of product and catalyst has hampered their practical application. As a result, heterogeneous catalysts are preferred due to their environmental friendliness, high selectivity, ease of recovery and reutilization, and adaptability to a variety of media [19-20]. The perennial challenge for researchers working on hydrogenation of glucose is to design a stable catalyst with high activity and selectivity. As such, the objective of this short review is to highlight the catalytic hydrogenation of glucose to sorbitol using Ru-based catalysts, as well as the reaction mechanism involved, given that Ru-based catalysts have been shown to have a high catalytic activity.

3. RECENT DEVELOPMENT OF RU-BASED CATALYST FOR HYDROGENATION OF GLUCOSE

3.1 Catalytic Activity of Ru-based Catalyst

Raney Ni catalysts are extensively used for sorbitol production; however, they present drawbacks such as Ni leaching and activity loss [21]. As an alternative to Ni-based catalysts, noble metals such as Ir, Rh, Pd, and Ru have been investigated as active phases in heterogeneous catalysts in the hydrogenation of glucose [22]. Ru demonstrated the highest catalytic activity and stability of all proposed active phases, resolving the issue of active phase leaching [23-24]. Ru metal is more expensive than Ni since it is a noble metal; consequently, Ru has been coated over several solid supports to minimise the final cost of the catalyst. Numerous studies have previously been conducted on Ru on activated carbon (AC) [25], silica [26], titanium dioxide (TiO_2) [27], NiO-modified TiO_2 [28], zeolites [29], and ordered mesoporous silica, MCM-41 [30], and MCM-48 [31].

Mishra et al. [28] investigated the effect of catalytic activity over HY zeolite supported Ru nanoparticles catalysts. Even after 10 hours of reaction time, no conversion of D-glucose was recorded as shown in Table 2, demonstrating Ru is the active metal centre in D-glucose hydrogenation. Ru/HYZ gave the highest D-glucose conversion compared to Ru/NiO-TiO_2 and Ru/TiO_2 with 19.4, 18.3 and 17.1%, respectively. When the response time was prolonged to 2 hours, the D-glucose conversion and sorbitol selectivity increased significantly. However, the reading started to decrease when 1.2 g of catalyst was used due to the increasing of by-product, D-mannitol formation. This demonstrated that 1.0 g of catalyst was adequate to achieve the maximum product selectivity (98.7%) and complete D-glucose conversion.

The catalytic activity of alumina silica-supported Ru materials depends on several factors including Ru oxidation state and synergistic effect between approximate Ru region and acid regions. Ru/TiO_2 with a metal loading around 1 wt.% was reported previously, showing high selectivity to sorbitol production around 93 %, at 120 ºC, 5.5 MPa H_2 and 120 min [32]. They observed a significant increase of the selectivity to sorbitol up to 97 %, after the modification of TiO_2 by impregnation nickel chloride and the following calcination (Ru/NiO-TiO_2, 1 wt % Ru). Zhu and his co-workers investigated on the ruthenium catalyst supported with a sulfonic acid functionalized silica (Ru/SiO_2–SO_3H) and Ru/SiO_2 for hydrogenolysis of cellulose into sorbitol and found that when using only sulfonic acid functionalized silica, a glucose yield of 56.6% was achieved, but sorbitol was not seen due to the lack of hydrogenation sites [26]. Meanwhile, the Ru/SiO_2 catalyst converted 36.2% of cellulose, but no sorbitol was produced. The bifunctional Ru/SiO_2–SO_3H catalyst revealed superior catalytic activity, converting 90.5% cellulose to sorbitol, and yielding 61.2% sorbitol. They specifically indicated a strong synergistic interaction between approximate Ru region and acid region in the conversion of cellulose to sorbitol.

An earlier study on hydrogenation of D-glucose using a Ru nanoparticles supported amine functionalized nanoporous polymer (AFPS) catalyst found that increasing Ru content in Ru/AFPS catalysts enhanced the formation of desired D-sorbitol, and 5Ru/AFPS catalyst (5 wt% of Ru) showed higher conversion and high D-sorbitol selectivity (98%) [33]. In comparison to non-functionalized polymer supported Ru catalyst (5Ru/PS), the catalyst 5Ru/AFPS exhibited higher catalyst performance. D-glucose isomerization is favoured by low Ru, resulting in more D-fructose while higher Ru catalysts promote D-glucose hydrogenation to produce D-sorbitol. Increased Ru content improved D-sorbitol selectivity, leading to a higher yield.

ZSM-5 zeolites with an adequate acidity and shape selectivity are frequently used as supports in hydrogenation processes [29]. They discovered that Ru/ZSM-5-TF (Ru species in ZSM-5 catalysts prepared via the latter approach) demonstrated significantly higher activity and selectivity than Ru/ZSM-5-MS (commercial microporous ZSM-5 zeolites with Si/Al = 38) and Ru/ZSM-5-AT (alkali-treated ZSM5 samples) (Si/Al = 38), with over 99% of D-glucose conversion and selectivity for D-sorbitol. The high performance of the catalyst can be described in term of bifunctional catalysis because of the presence of both acidic (support) and basic (metal) sites on the surface.

MCM-48 possessed an ordered cubic structure based on a narrow tridimensional pore and was used as one of the reaction's support materials [31]. Romero and his co-workers observed that the catalytic activity of Ru/MCM-48 remained constant and the yield of sorbitol was 90% after three cycles of hydrogenation reaction. The optimal temperature range for this reaction was 80-120 °C, as they

noticed that when the reaction temperature exceeded 120 °C, the sorbitol yield decreased due to thermal degradation of D-glucose and isomerization of sorbitol into mannitol. Additionally, they conducted a comparative study with the Ru/MCM-41 catalyst [30] and proved that Ru/MCM-48 exhibited the highest stability, which they attributed to the pore structure difference between the two catalysts, as MCM-48 has a cubic pore structure, whereas MCM-41 has a hexagonal array of unidirectional pores, which can result in additional diffusional limitations or pore blockage.

The effect of carbonized cassava dregs (CCD) supported on Ru catalysts on the conversion of D-glucose into D-sorbitol has been investigated and they discovered that as the carbonization temperature increased from 300 to 450 °C, the D-glucose conversion increased from 41.5 to 99.7% [25]. The same trend has been followed by the D-sorbitol yield where it showed an increment from 36.8% to 98.6%. Both glucose conversion and sorbitol yield decreased significantly when carbonization temperatures reached 500 °C, indicating a high carbon content in the carbonized cassava dregs, which may have resulted in a reduction in Ru metal binding sites. Other than that, Ru/AC catalyst also demonstrated excellent catalytic performance, with 100% glucose conversion and a sorbitol yield of 96.5%, suggested that the hydrogenation reaction occurred rapidly at a moderate temperature of 120 °C in the presence of Ru metal. In a comparison study with Pt/CCD, they noticed that lower sorbitol yield (93.3%) was recorded even though the glucose was completely converted, showing that Ru exhibited higher catalytic performance compared to Pt for this reaction.

Recently, a study done by Musci et al. [24] on the activity and selectivity of Ru catalysts supported on various materials, including gamma alumina (A), zirconia (Z), zirconia-alumina (Z-A), phosphate zirconia (ZP) and phosphate zirconia-alumina (ZP-A). The catalytic activity of these catalysts ranged in ascending order of glucose conversion: Ru/ZP < Ru/A < Ru/Z < Ru/Z-A < Ru/ZP-A. The size of the metallic particles and the properties of the support appear to play major roles in boosting the activity of the catalysts. Based on transmission electron microscopy (TEM) results, Ru/Z-A catalyst contained smaller Ru particles with 1.42 nm compared to Ru/ZP-A catalyst with 3.08 nm. According to Ruppert et al. [34], Ru particles smaller than 1 nm would be trapped in the support pores, decreasing their availability for the reaction. Thus, the literature reports corroborated their observations and proved that the most active catalyst was Ru/ZP-A which gave 97% of sorbitol selectivity with less amount of mannitol by-product.

3.2 Reaction Mechanisms

Nowadays, practically all sorbitol manufacturing procedures are based on the hydrogenation of glucose using metallic catalysts. Currently, this industrial process is dominated by the use of Raney Ni [4]. However, the technique is frequently ineffective and may contribute to environmental pollution as a result of Ni-Al alloy leaching. Amorphous alloys, which are thermodynamically non-equilibrium metastable materials having a long-range disordered but short-range ordered structure, have garnered increasing interest from academia and industry owing to its excellent catalytic properties when compared to their crystalline counterparts [35].

Yang et al. [36] recently synthesised a hollow Ni-P nanospheres (NSs) catalyst and tested the performance of the catalyst on sugars hydrogenation reaction. They reported that hollow Ni-P amorphous alloy NSs demonstrated much higher catalytic performance to the commercial Raney Ni catalyst during liquid-phase hydrogenation of sugars to sugar alcohols, indicating a greater potential for practical applications. The high catalytic activity indicated that the hollow Ni materials with a nano porous chamber structure had several advantages, including ease of experimental handling and high accessibility for reactants in liquid-phase reactions, increased Ni active sites, and the presence of a more electron-rich inner surface, all of which are necessary for the development of highly efficient catalysts for certain processes. A model that illustrates the adsorption and hydrogenation of glucose on the inner surface of Ni-P-H can be depicted in Scheme 2. It is therefore expected that more electron-rich Ni active sites on the inner surface of Ni-P-H will be able to efficiently remove proton from glucose. However, the greater electron density on Ni active sites may stimulate the production of H species, which could enhance glucose hydrogenation performance.

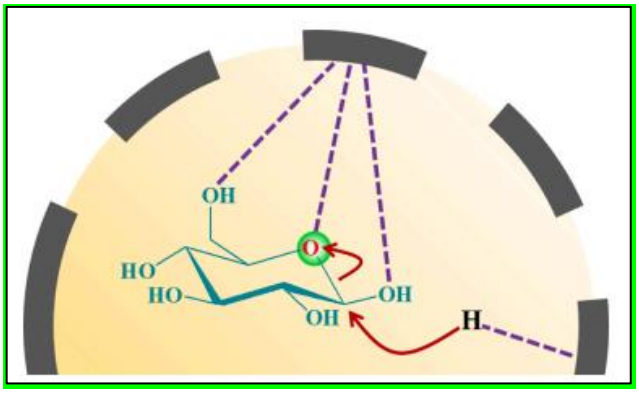

Scheme 2: Graphical illustration of the reaction mechanism between adsorbed glucose and hydrogen on Ni-P-H amorphous alloy catalyst [36].

A study on carbon black supported Ni (Ni/CB), Fe (Fe/CB) and Fe-Ni (FeNi/CB) alloy catalyst for glucose hydrogenation has been investigated by Fu et al. [37] and they found that Fe and Ni favour separate reaction routes while Fe-Ni alloy catalysts exhibited synergistic effects. The conversion of glucose and sorbitol yield were significantly increased when Fe and Ni formed an alloy. The catalytic conversion of glucose to sorbitol in the aqueous phase is schematically visualized in Scheme 3. The polarisation of

Table 2: Hydrogenation performance of glucose over different reaction conditions.

Catalyst	Temperature (°C)	Time (h)	Catalyst amount (g)	Percentage of solution and catalyst (%)	Pressure (MPa)	Glucose Conversion (%)	Product selectivity (%)				Ref.
							D-Sorbitol (SB)	D-Mannitol (MN)	D-Fructose (FR)	Others	
HYZ	120	0.3	-	D-glucose = 40 g	5	-	-	-	-	-	[28]
Ru/HYZ	120	0.3	1.0	D-glucose = 40 g Ru = 1	5	19.4	97.6	-	-	-	[28]
Ru/HYZ	120	2	1.0	D-glucose = 40 g Ru = 1	5	100	98.7	0.7	-	Non identified products = 0.6	[28]
Ru/HYZ	120	2	1.2	D-glucose = 40 g Ru = 1	5	100	98.5	1.0	-	Non identified products = 0.5	[28]
Ru/NiO-TiO_2	120	0.3	1.0	D-glucose = 40 g Ru = 1	5	18.3	96	-	-	-	[28]
Ru/AFPS	100	1	0.1	D-glucose = 11.10 mmol Ru = 1	5.5	15	94	3	2	Non identified products = 1	[33]
Ru/AFPS	100	1	0.1	D-glucose = 11.10 mmol Ru = 2	5.5	31	96	2	1	Non identified products = 1	[33]
Ru/AFPS	100	1	0.1	D-glucose = 11.10 mmol Ru = 3	5.5	50	98	1.0	0.5	Non identified products = 0.5	[33]
Ru/AFPS	100	1	0.1	D-glucose = 11.10 mmol Ru = 5	5.5	69	98	1.5	-	Non identified products = 0.5	[33]
Ru/ZSM-5-TF	120	2	0.5	D-glucose = 50 g Ru = 1	4	99.6	99.2	-	-	-	[29]
Ru-MCM-41	120	2	-	D-glucose = 10 Ru = 3.98	3	100	83.13	-	-	-	[30]
Ru-MCM-48	120	0.4	-	D-glucose = 7.35 g/dm^3 Ru = 4.04	2.5	89.56	89.56	-	-	-	[31]
Ru/TiO_2	120	0.3	-	D-glucose = 7.35 g/dm^3 Ru = 3.98	2.5	91.39	91.39	-	-	-	[31]
Ru/C	120	0.2	-	D-glucose = 7.35 g/dm^3 Ru = 5	2.5	94.75	94.75	-	-	-	[31]
Ru/AC	120	1.5	1.0	D-glucose = 10 Ru = 5	3	100	96.5	-	-	-	[25]
Ru/CCD	120	1.5	1.0	D-glucose = 10 Ru = 5	3	99.7	98.6	-	-	-	[25]
Pt/CCD	120	1.5	1.0	D-glucose = 10 Ru = 5	3	100	93.3	-	-	-	[25]
Ru/A	90	7	25	D-glucose = 0.9 g Ru= 3	1.25	33	100	-	-	-	[24]
Ru/Z	90	7	25	D-glucose = 0.9 g Ru= 3	1.25	42	99	-	-	-	[24]

the C=O bond then facilitates the nucleophilic addition of hydrides (H adatoms) on the metal surface, resulting in the formation of sorbitol. They concluded the Ni-based catalyst was deactivated due to particle development, surface oxidation, and leaching, whereas the Fe-Ni alloy catalyst demonstrated obvious stability advantages over the monometallic Ni catalyst.

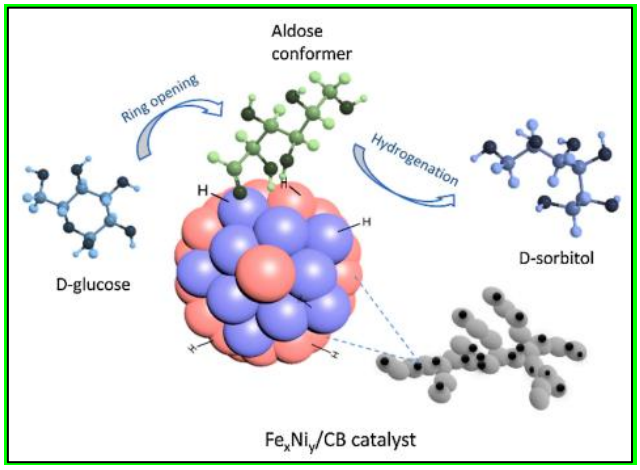

Scheme 3: Fe_xNi_y alloy catalysts supported on carbon black for aqueous-phase hydrogenation of glucose to sorbitol [37].

These Ni-based catalysts demonstrated strong catalytic activity despite their high H_2 pressure need and lower selectivity for D-sorbitol. Additionally, the need for special care while handling Raney Ni, the leaching of Ni, and the ease with which catalysts can be deactivated are significant difficulties with Ni-based catalysts. Among the metal catalysts investigated, it was discovered that supported Ru catalysts were more active and selective than Raney Ni catalyst. Ru-based catalysts functioned at a lower H_2 pressure, exhibited no leaching, less sensitive to deactivation, and are recyclable [38]. Zhang et al. [30] described the molecular process for the conversion of glucose to sorbitol utilising Ru/MCM-41 as a catalyst. On the basis of Scheme 4, it has been presumed that H_2 absorbs and activates on the active sites of the catalysts before reacting with the glucose carbonyl group. As a consequence of the irreversible reaction between glucose and activated hydrogen (H^+) on the catalyst surface, sorbitol is produced as the final liquid phase product. The hydrogenation of glucose on a Ru/MCM-41 catalyst is a multistep process that begins with hydrogen dissolution and diffusion in the reaction media, followed by its absorption on the catalyst surface, activation, and lastly interaction with the carbonyl group on glucose to form sorbitol [39].

Zhao et al. [2] reported that a core-shell-like sphere ruthenium catalyst, identified as 5%Ru/γ-Al_2O_3@ASMA, has been successfully synthesized through impregnating the ruthenium nanoparticles (NPs) on the surface of the amino poly (styrene-co-maleic) polymer (ASMA) encapsulating γ-Al_2O_3 pellet support. The 5%Ru/γ-Al_2O_3@ASMA is

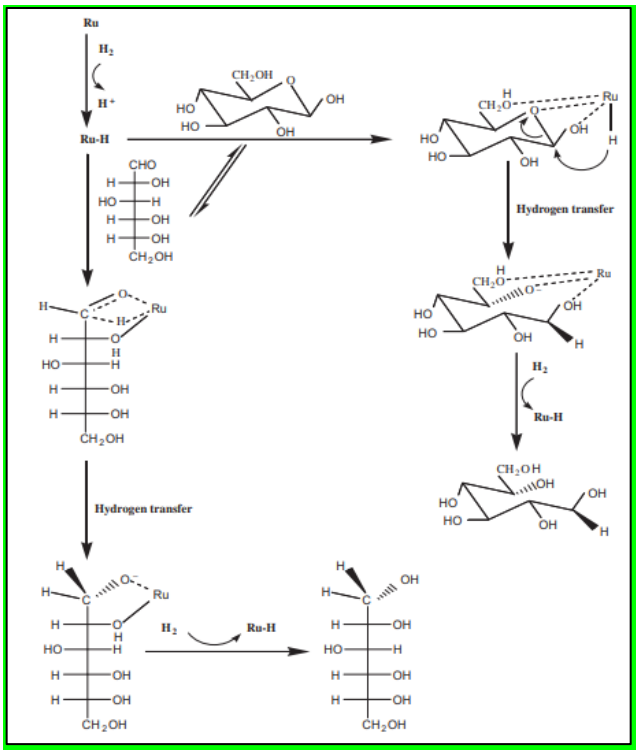

Scheme 4: Mechanism of glucose hydrogenation over Ru/MCM41 [30].

effective for glucose hydrogenation and exhibited a consistent sorbitol yield of over 90% in both batch and trickle bed reactors, showing the potential practicality of the core-shell-like catalyst for efficient sorbitol production. H_2 was first adsorbed on the uniformly scattered Ru catalytic sites to create the active hydrogen species during the hydrogenation process. As soon as the active hydrogen combines with glucose molecules, it attacks the carbonyl groups of the reactant, and the target sorbitol can be produced and desorbed into the mixed solution as shown in Scheme 5. Since the exterior -OH and -NH_2 on the ASMA shell form strong hydrogen bonds, as opposed to the pure van de Waals force between Ru NPs and the γ-Al_2O_3 pellet, it is possible to bind the Ru NPs to the support much more strongly. The strong interaction between Ru NPs and ASMA encapsulating γ-Al_2O_3 would further enhance the catalyst's recyclability.

As discussed in earlier section, the hydrogenation of D-glucose to D-sorbitol was shown to be highly efficient using Ru/AFPS catalysts [33]. The catalyst containing 5%wt Ru (5Ru/AFPS) demonstrated high D-glucose conversion and selectivity (98%). The hydrogenation of D-glucose to D-sorbitol using a Ru catalyst supported by AFPS is a three-phase catalytic reaction (gas–liquid–solid). It has been demonstrated that Ru placed on mesoporous polymeric supports can adsorb more H_2 than the metal itself via hydrogen spillover. According to this approach, the

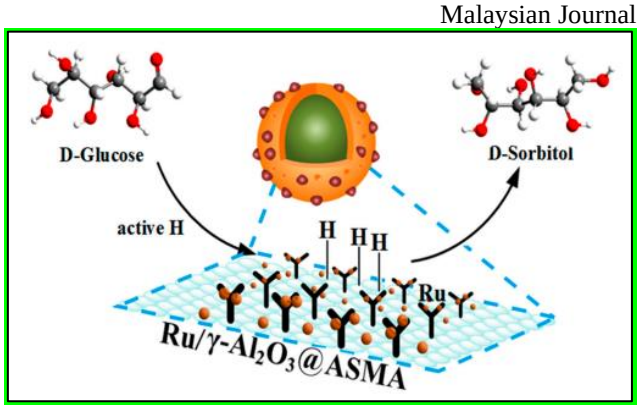

Scheme 5: The hydrogenation route from glucose to sorbitol using 5%Ru/γ-Al_2O_3@ASMA pellet as catalyst [2].

progression of D-glucose hydrogenation can be explained by H_2 diffusion, the production of activated hydrogen (H-Ru), and the reaction of D-glucose with active hydrogen on the catalyst surface. The proposed process for D-glucose hydrogenation employing a Ru/AFPS catalyst is detailed in Scheme 5. Hydrogen is transmitted from air to liquid and then dissolved at the gas–liquid interface during the hydrogenation of D-glucose to D-sorbitol. The dissolved hydrogen in the liquid phase then spills over onto the catalyst surface, where it is activated by the catalyst's active metal (Ru) centres. D-carbonyl glucose's group combines with activated H and Ru to form a cyclic transition structure. The hydrogen transfer then occurs, and the addition of H_2 results in the formation of active H and the product D-sorbitol. D-sorbitol diffuses into the liquid phase after desorbing from the catalyst. The freshly formed active hydrogen can then be used to convert another molecule of D-glucose, and the hydrogenation cycle can continue. The results indicated that a catalyst nano porous structure with a diverse range of pores, a high specific surface area, and the presence of functional groups on the surface played a critical role in improving the catalyst's performance.

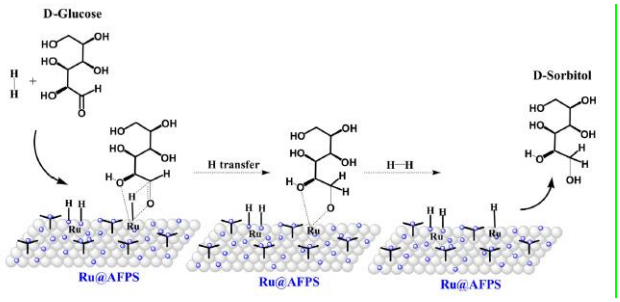

Scheme 6: The reaction mechanism proposed for D-glucose hydrogenation to D-sorbitol using a 5Ru/AFPS catalyst [33].

3.3 Catalyst Deactivation

Although the hydrogenation of D-glucose to D-sorbitol appears straightforward, in practise, D-glucose is converted not only to a single product, d-sorbitol, but also to a variety of different by-products, as illustrated in Scheme 1. Some of the by-products are generated via non-catalytic pathways. The commercial manufacture of sorbitol is facilitated by the stability of the catalyst used in the glucose hydrogenation process. Sintering and catalyst poisoning are two drawbacks that should be prevented. Apart from that, metal leaching must be minimised, as it clogs active sites and limits the use of sorbitol in food and medicine. Table 3 summarised the previous studies on the reusability of different heterogenous catalysts for hydrogenation of glucose.

Guo et al. [29] efficiently reused Ru/ZSM-5-TF for glucose hydrogenation for five trials under the same reaction conditions (4% catalyst ratio, 4 MPa H_2, 2 h, 220 °C). They observed that the catalyst recorded high glucose conversion and sorbitol selectivity in all cycles. The reaction liquid remained colourless after filtration and almost no Ru leaching was detected by ICP. No aggregation of Ru nanoparticles was observed using TEM images. They claimed that the reduction of glucose conversion from 99.7 to 88.2% after the fifth run could be a result of the regeneration method used, but the spent catalyst showed no obvious loss of the catalytic activity after being washed with water, ethanol, or acetone for three times each. Thus, deactivation could be induced by an accumulation of organic and inorganic species adsorbed on the surface of the catalyst.

The sufficient stability of supported Ru catalysts was also demonstrated by Mishra et al. [28] for hydrogenation of glucose over Ru/HYZ catalyst. They reported that within four cycles, the glucose conversion rate dropped from 100 to 94%, and the sorbitol selectivity dropped from 98 to 94%. As a result, the catalyst is capable of being reused up to four times without losing its activity. According to the TEM images shown in Figure 3, both fresh and spent catalysts exhibited no perceptible morphological changes following four runs. The high catalyst stability revealed the strong interaction between the active Ru species and the HY zeolite support.

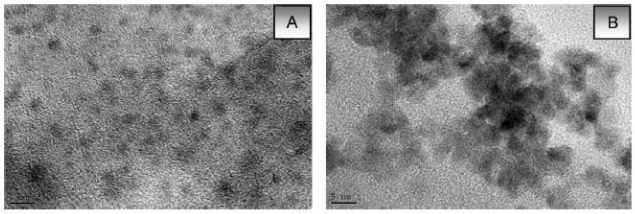

Figure 2: TEM images of (A) fresh catalyst and (B) spent catalyst after four runs [28].

Dabbawala et al. [33] conducted another reusability study on glucose hydrogenation using Ru/AFPS under optimised conditions and found that only 2% glucose conversion was reduced (from 68 to 66%) after fifth cycles. Due to the absence of Ru leaching into the reaction mixture, the catalyst is reusable for up to five cycles under the reaction conditions used. Some additional peaks were detected in the FTIR spectra of used catalysts which could be attributed to the adsorption of substrate or/and product molecules. The TEM images revealed no changes in the

morphology of the catalyst. A small amount of Ru nanoparticle aggregation was identified, which may account for the slight decrease in catalyst performance observed with spent catalysts. The observation established that the catalyst is sufficiently stable during the reaction due to the strong interaction between Ru metal and AFPS support, which is encouraging for sugar-to-sugar alcohol conversion.

Table 3: Reusability studies using various catalysts for glucose hydrogenation.

Catalyst	Number of Cycles	Conversion of glucose (%)	Ref.
Ru/HYZ	4	100-94	[28]
Ru/ZSM-5-TF	5	99.7-89.2	[29]
Ru/AFPS	5	68-66	[33]

4. CONCLUSION AND FUTURE PERSPECTIVE

The hydrogenation of glucose into sorbitol over Ru-based catalysts was reviewed. Briefly, different catalytic performances were obtained depending on the catalysts used, and the data proved that more than 80% sorbitol yield was achieved when Ru-based catalysts were used in this reaction. It was shown that the catalyst-to-glucose ratio or metal loading factor had a substantial effect on hydrogenation performance in relation to reaction time and temperature. Increases in reaction time and temperature significantly improved glucose conversion. The sorbitol yield or selectivity may be reduced because of glucose or sorbitol degradation. Also, the supported Ru catalyst demonstrated a little reduction in sugar conversion across many reuse cycles. Thus, supported Ru catalysts were proved to be the most efficient reusability for glucose hydrogenation to sorbitol.

Numerous studies have been conducted into the use of heterogeneous catalytic hydrogenation to produce sorbitol from monosaccharides such as glucose, and highlighted its advantages, including its flexibility, high efficiency, and environmental friendliness. However, significant goals have yet to be met. For instance, synthesising a catalyst with environmentally friendly, non-toxic, high stability, and selectivity towards a target product. Additionally, more cost-effective sorbitol synthesis under low to moderate operating parameters (time, temperature, pressure, and amount of catalyst) is a challenge that must be overcome. Other than that, in order to obtain a high-purity product, the separation of sorbitol from residual glucose or other by-products formed should be resolved.

ACKNOWLEDGEMENTS

This work was supported by Fundamental Research Grant Scheme (FRGS/1/2018/STG 07/UITM/02/23) from Ministry of Higher Education, Malaysia and Geran Penyelidikan Bestari Phase 2/2021 from Universiti Teknologi MARA, Cawangan Johor.

REFERENCES

[1] Economic Planning Unit (EPU) (2019). Twelfth Malaysia Plan, 2021-2025. Putrajaya.
[2] J. Zhao, X. Yang, W. Wang, J. Liang, Y. Orooji, C. Dai, X. Fu, Y. Yang, W. Xu, J. Zhu, Catal. 10 (2020) 1068.
[3] M. Zheng, A. Wang, J. Pang, N. Li, T. Zhang, Editors, Springer Singapore: Singapore, 2016, p. 227-260.
[4] B. Garcia, J. Moreno, G. Morales, J.A. Malero, J. Iglesias, Appl. Sci. 10 (2020)1843.
[5] S. Wang, W. Wei, Y. Zhao, H. Li, H. Li, Catal. Today. 258 (2015) 327-336.
[6] C. Marques, R. Tarek, M. Sara, K. Brar, Platform Chemical Biorefinery, Elsevier, 2016, p. 217–227.
[7] M. Grembecka, Eur Food Res Technol. 241 (2015) 1–14.
[8] V.G. Matveevaa, V.N. Sapunovb, M.E. Grigor'ev, M.B. Lebedevaa, E.M. Sul'man, Kinet. Catal. 55(6) (2014) 695-704.
[9] N.S. Hassan, A.A. Jalil, C.N.C. Hitam, D.V.N. Vo, W. Nabgan, Environ. Chem. Lett. 18 (2020) 1625–1648.
[10] M.J. Ahmed, B.H. Hameed, J. Taiwan Inst. Chem. Eng. 96 (2019) 341-352.
[11] A. Shendurse, C.D. Khedkar, Glucose: Properties and Analysis. The Encyclopedia of Food and Health, 3. Oxford: Academic Press, 2016, p. 47-239.
[12] G. Sampath, K. Srinivasan, Appl. Catal. A-Gen. 533 (2017) 75–80.
[13] S. Schimpf, C. Louis, P. Claus, Appl. Catal. A-Gen. 318 (2007) 45-53.
[14] D.K. Mishra, J.S. Hwang, Appl. Catal. A-Gen. 453 (2013) 13-19.
[15] S. De, R. Luque, Nanomaterials for the Production of Biofuels, in Nanomaterials for Sustainable Energy, Q. Li, Editor, Springer International Publishing: Cham, 2016, p. 559-582.
[16] J. Su, J.S. Chen, Micropor. Mesopor. Mat. 237 (2017) 246–259.
[17] J.K. Nørskov, F. Studt, F. Abild-Pedersen, T. Bligaard, Fundamental Concepts in Heterogeneous Catalysis. Hoboken, NJ, USA: John Wiley & Sons, Inc, 2014, p. 2.
[18] I. Thapa, B. Mullen, A. Saleem, C. Leibig, R.T. Baker, J.B. Giorgi, Appl. Catal. A-Gen. 539 (2017) 70–79.
[19] L.S. Ribeiro, J.J. Delgado, J.J. de Melo Órfão, M.F.R. Pereira, Catal. Today. 279 (2017) 244–251.
[20] Y. Zhang, T. Chen, G. Zhang, G. Wang, H. Zhang, Appl. Catal. A-Gen. 562 (2018) 258–266.
[21] A. Malinovskya, V. Matveevaa, E. Sulmana, V. Doludaa, A. Stepachevaa, E. Rebrova, Chem. Eng. Trans. 61 (2017) 613-618.
[22] A. Negoi, K. Triantafyllidis, V.I. Parvulescu, S.M. Coman, Catal. Today. 223 (2014) 122–128.

[23] M. Almohallaa, I. Rodríguez-Ramosb, L.S. Ribeiroc, J.J.M. Órfãoc, M.F.R. Pereirac, A. Guerrero-Ruiz, A. Catal. Today. 301 (2018) 65-71.
[24] J.J. Musci, M. Montañac, E. Rodríguez-Castellónd, I.D. Lickc, M.L. Casellaa, Mol. Catal. 495 (2020) 111150.
[25] Z. Li, Y. Liu, S. Wu, Bioresources. 13(1) (2018) 1278-1288.
[26] W. Zhu, H. Yang, J. Chen, C. Chen, L. Guo, H. Gan, X. Zhao, Z. Hou, Green Chem. 16 (2014) 1534–1542.
[27] N. Perkas, Z. Zhong, L. Chen, M. Besson, A. Gedanken, Catal. Lett. 103(1-2) (2005) 9-14.
[28] D.K. Mishra, A.A. Dabbawala, J.J. Park, S.W. Jhung, J.S. Hwang, Catal. Today. 232 (2014) 99–107.
[29] X. Guo, X. Wang, J. Guan, X. Chen, Z. Qin, X. Mu, M. Xian (2014). Chinese J. Catal. 35 (2014) 733–740.
[30] J. Zhang, L. Lin, J. Zhang, J. Shi, Carbohyd. Res. 346 (2011) 1327–1332.
[31] A. Romero, E. Alonso, A. Sastre, A. Nieto-Marquez, Micropor. Mesopor. Mat. 224 (2016) 1-8.
[32] D.K. Mishra, J.M. Lee, J.S. Chang, J.S. Hwang, Catal. Today. 185 (2012) 104-108.
[33] A.A. Dabbawala, D.K. Mishra, J.S. Hwang, Catal. Today. 265 (2016)163–173.
[34] A.M. Ruppert, J. Grams, M. Jędrzejczyk, J. Matras-Michalska, N. Keller, K. Ostojska, P. Sautet, ChemSusChem. 8 (9) (2015)1538–1547.
[35] M. Wang, B. Feng, H. Li, H.X. Li, Chem, 5 (2019) 805.
[36] Y. Yang, H. Gu, Q. Zhang, F. Zhang, H. Li, Catal. Today. 365 (2021) 282-290.
[37] Y. Fu, L. Ding, M.L. Singleton, H. Idrissi, S. Hermans, Appl. Catal. B. 288 (2021) 119997.
[38] J.G.A.B. Silva, R.C. Santos, E. Rodríguez Castellon, L.S.G. Teixeira, L.A. M. Pontes. Mol. Catal. 507 (2021) 111567.
[39] B. Zada, M. Chen, C. Chen, L. Yan, Q. Xu, W. Li, Q. Guo, Y. Fu, Sci China Chem. 60 (2017) 1-17.

Malaysian Journal of Catalysis
http://mjcat.utm.my/
MJCat
Research Article

Development of zeolites for zeoforming reaction of naphtha

Walid Nabgan[a, b*], Bahador Nabgan[a, b], Tuan Amran Tuan Abdullah[a,b], Mohamad Wijayanuddin Ali[a,b]

[a] *School of Chemical and Energy Engineering, Faculty of Engineering, Universiti Teknologi Malaysia, 81310 Skudai, Johor, Malaysia.*
[b] *Centre of Hydrogen Energy, Institute of Future Energy, Universiti Teknologi Malaysia, 81310 Skudai, Johor, Malaysia.*

**Corresponding Author: wnabgan@gmail.com,*

Article history:
Received 16 August 2021
Accepted 4 October 2021

ABSTRACT

High octane naphtha production is the primary purpose of the zeoforming process that is genuinely needed in our modern life. Sulfur-containing compounds in gasoline are causing environmental pollution and catalysts deactivation. The metal function supplied by non-noble promoters such as Fe, Mn, Ni, Co, Cu, and Zn is deposited on the ZSM-5 type of zeolite. ZSM-5 zeolites were prepared by successive hydrothermal treatment following by impregnation of promoters on ZSM-5 type zeolite. The catalysts were characterized, utilizing XRD, N_2 physisorption, FESEM, TEM, TPR-H_2, and TPD-NH_3. Bibliometric results show that feed conversion concerns are the primary focus in naphtha and zeolite topic studies. Particular attention has been paid to ZSM-5 and performance that may be crucial for improving the naphtha reforming reaction. The experimental results verified that different promoters' use has a profound effect on zeolites' physicochemical properties. It found that Fe interacts strongly with the ZSM-5 zeolite producing growth in the metal function activity. The zeoforming results indicate that the highest research octane number (RON) belonged to the Fe promoter. A Fe promoter's existence increased the stability and selectivity for C_{7+} isomers and aromatics, thus reducing the formation of sulfur and low-value products like methane and gases.

Keywords: Non-precious metal; bibliometric; ZSM-5; zeoforming reaction; naphtha

| eISSN 0128-2581 |

1. INTRODUCTION

Refineries must also manufacture sustainable goods to comply with the strict global regulations surrounding air emissions. One of the primary sources of achieving human necessity for energy is fossil fuels, accompanied by pollutant agents such as sulfur that are not environmentally sustainable and may cause serious public health problems when inhaled or exposed. New sulfur part common values, as well as the octane number in gasoline, have been developed. Sulfur-containing compounds in fuel are linked to SOx and particulate matter (PM) emissions from gasoline generators, which cause contamination and acid rain in the environment. During the burning or fermentation of fuels, sulfur can be converted to other sulfurous compounds such as SO_2 and H_2S. The intense need to preserve the living ecosystem supports the publication of rigorous pollution legislation and prohibits harmful organisms (S, aromatics, and polyaromatics) in fuel requirements. According to the new regulations, industrial units must limit sulfur yields to no more than 10 mg/kg and raise RON values to at least 90. As a result, the operating units must quickly adjust their products to the new requirements [1]. Consequently, it is critical to consider starting a long-term strategy for reducing the negative effects of fuels to achieve an environmentally friendly process.

The sulphur portion in gasoline was eliminated from the feedthrough hydrodesulfurization (HDS) method before the octane number enrichment process. In the manufacturing sector, HDS is one of the methods for removing sulfur from petroleum products. New inexpensive and effective strategies for desulfurization of refractory organic sulfur are needed by strict new legislation to reduce sulfur content in fossil fuels. There are significant research efforts have been dedicated to improving the HDS process by developing bimetallic and trimetallic catalysts [2-13] to stop radioactive waste in the atmosphere and contamination of the transforming catalyst as a result of the reaction. HDS of such substances is very expensive and necessitates high temperatures and pressures during operation [14]. Other

scientists employed zeolite to strip sulfur from naphtha as a catalyst. For instance, Sharifi et al. [1] produced the W/HZSM-5 catalyst for octane improvement and desulfurization at the same time. They discovered that the catalyst with a SiO_2/Al_2O_3 ratio of 60:1 had the most excellent output in the corresponding octane improvement phase. Sulfur compounds were reduced by 67.5 percent, and octane increased by 90 percent. Sulfur components in naphtha, on the other side, prove to be a cause of catalyst deactivation and high-octane fuel output concerns. Non-noble metals, such as Ni, Fe, Mn, Co, Cu, Zn, have been deposited onto W-HZSM-5 as a conventional metal in HDS industrial catalysts [15]. According to some studies, the ZSM-5 catalyst is highly effective at aromatizing and upgrading gasoline [1, 16-19]. As a result, the benefits of zeolite as a catalyst for the zeoforming phase with non-noble metals are its environmental friendliness and sulfur activity. According to these studies, the collaboration between acid zeolite catalysts like ZSM-5 and non-precious metals as promoters could significantly increase the sequential desulfurization-aromatization process performance.

In this context, it is clear that there is no consensus in the literature on the zeoforming process. This process is crucial for adequately planning future research designs but is currently unavailable. In our previous research [20], we sincerely reviewed hydrodesulfurization, catalysts used for the naphtha reforming process, and how the zeoforming process would decrease the sulfur component without using the conventional hydrodesulfurization process. There is no paper has been published on promoters' impact on the catalytic behavior of the zeoforming reaction, as far as we know. Thus, this study aims to systematically examine reports of "naphtha" and "zeolite" and the primary trend and focus of research from 1970 to 2021, containing journals, research topics, widely quoted articles, and often used keywords; and to determine the effect of non-noble metal promoters on the properties of the acid and metal functions of ZSM-5 type zeolite for zeoforming reaction. The zeolites synthesized in this study have been characterized through XRD, N_2 physisorption, FESEM, TEM, TPR-H_2, and TPD-NH_3 analysis. The catalysts' catalytic behavior has been explained accordingly, and the proposed reaction mechanism of the zeoforming process was drawn.

2. EXPERIMENTS

It started with a bibliographical quest in the WOS directory of periodicals. A few keywords were used to conduct this research, and these keywords were incorporated into the WOS search engines by following the form of the Boolean "AND". The program EndNotes X 5TM was used to index these archives, and the raw research was kept there. Accordingly, bibliometrics was carried out using the mathematical study of publication peaks and keyword networking. The experimental study was carried out in line with the pattern in experiments and study void found.

2.1 Catalyst preparation

The synthesis of ZSM-5 zeolite was performed from a sol-gel intermediate with the chemical compositions of Al_2O_3: 120 SiO_2: 3 TPAOH:6 TPABr: 1.5 Na_2O: 1000 H_2O in the following order and using a hydrothermal treatment which also described elsewhere [21, 22]. Initially, NaOH pellets and aluminum isopropylate were melted in distilled water (solution I), supplemented by distilled water with a measured amount of TPAOH and TPABr (solution II), and finally, distilled water with a source of silica (solution III). To achieve homogeneity, each solution was stirred for 4 hours. Then, the solutions (I) and (II) were added drop-wise to the solution (III) under dynamic mixing. The resulting mixture was blended for 12-16 h at room temperature to ensure homogeneity. The synthesized gel was transferred into a stainless-steel autoclave hydrothermal reactor with PTFE lining (200 mL) and maintained at an appropriate temperature of 150 ^oC for 48 h. The solid stock was purified and washed with deionized water until the washing water's pH hit 6, then dried for 24 hours at 110 ^oC. The outcome was calcined for 5 h at 600 ^oC. Using the impregnation technique, the promoters/ZSM-5 catalysts (all elements from Aldrich) were developed. The impregnation process has the benefit of producing a large concentration of active substances on the catalyst surface. [23, 24]. To prepare the catalysts, 1 wt.% non-noble promoters such as Fe, Ni, Co, Cu, Zn, and Mn with 99 wt.% of ZSM-5 were mixed in 200 mL deionized water. The mixture was heated to 90 °C and mixed with a hot plate until it thickened into a viscous paste. The paste was cured overnight in an oven at 110 °C. The catalyst was then calcined at 600°C overnight in a furnace before being cooled to room temperature. The mixture was heated to 90 °C and mixed with a magnetic stirrer until it became an extremely viscous paste. The paste was cured overnight in an oven at 110 °C. The catalyst was then calcined at 600 °C overnight in a furnace before being cooled to room temperature. Prepared ZSM-5 samples are shown in Figure 1 and were named Fe/ZSM-5, Ni/ZSM-5, Co/ZSM-5, Cu/ZSM-5, Zn/ZSM-5, and Mn/ZSM-5. Samples were grinded and fermented on 2 phases of 35 and 34 mesh before the experiment reaction test to achieve particles with a scale of 1.0 mm to 1.4 mm.

Figure 1 Prepared ZSM-5 samples with different promoters

2.2 Catalyst characterization

The X-ray diffraction (XRD) of the samples was carried out on an X-ray diffractometer by Ni filtered Cu K α radiation with a scanning angle (2θ) of 5 to 80° with a step size of 0.02° and a step time of 49 s. Furthermore, the Brunauer–Emmett–Teller (BET) procedure was extended to the isotherms of N_2 adsorption to measure reduced catalyst entire surface region, estimated at liquid nitrogen temperature on a Beckman Coulter SA3100^{TM} apparatus at 200 °C for 2 h on outgassed samples. A JEM-ARM200F microscope was used for transmission electron microscopy (TEM). The acidity of the formulated catalysts was calculated using a Micromeritics Chemisorb 2720 chemisorption analyzer. To determine the total acidity of catalysts, 35 mg of the sample was kept at 600 °C for 60 minutes under a 30 mL/min argon flow rate, then cooled to 25 °C and held under a 20 mL/min helium flow rate for 30 minutes. The catalyst was saturated with NH_3 for 30 minutes at a rate of 20 mL/min in argon containing 5% (vol.) NH_3.

2.3 Zeoforming reaction

There have been many approaches for designing the reactor and processes comparable to other catalytic materials production. We previously demonstrated that fluid bed reactors could accommodate massive feed and catalyst volumes in a previous study [20]. On the other hand, fixed bed reactors were extensively used in earlier tests of the catalytic reforming mechanism with strong catalysts. The fixed bed reactor is the most popular method for studying gas-phase reactants with a strong catalyst to synthesize large quantities of appropriate chemicals and intermediates [25, 26]. Fixed-bed reactors have been primarily used for the disposal of radioactive and hazardous compounds in recent years, in addition to the synthesis of valuable chemicals [25]. The experimental setup for the zeoforming process is depicted in Figure 2. A total of 0.1 g of catalyst was included in the activity samples. The catalyst bed was installed in a 0.5-inch OD quartz tubular reactor with a coaxially focused thermocouple. Before the reaction, the catalyst bed was flooded with nitrogen at 300 °C, then reduced in situ for 1 hour at 600 °C with 30 mL/min pure hydrogen. As n-heptane is a significant component in naphtha, it was chosen as a typical feed for this set of experiments to give a realistic picture of the industrial reforming process [27]. Until combining with carrier N_2, N-heptane was fed separately into the pre-heater using an HPLC pump (Bio-RadTM, Series 1350) at 0.1 mL/min. At a temperature of 400 °C and a pressure of 10 bar, the reduced materials were checked for n-heptane. The reaction last for an hour and stability test last for 24 continues hours for the optimum catalyst. The reaction products were studied using a GC with TCD (Agilent 6890N) and a Carboxen Plot 1010 capillary column (Fused silica, 30 m x 0.53 mm) attached in sequence argon as the carrier gas. Meanwhile, a GC-FID with a Petrocol-DH column (100 m 0.25 mm ID) and a flame ionisation detector are used to test the liquid product. By utilizing specific solutions and the table included with the panel, the peaks in the chromatograms received from the GC were established. In each catalytic experiment, the study octane number (RON) for the finished product was determined as:

$$RON = \sum_{i=1}^{K} y_i RON_i$$

where RONi represents the analysis octane amount of each pure ingredient i in the end product, and y_i represents the mole fraction of particle i [28, 29].

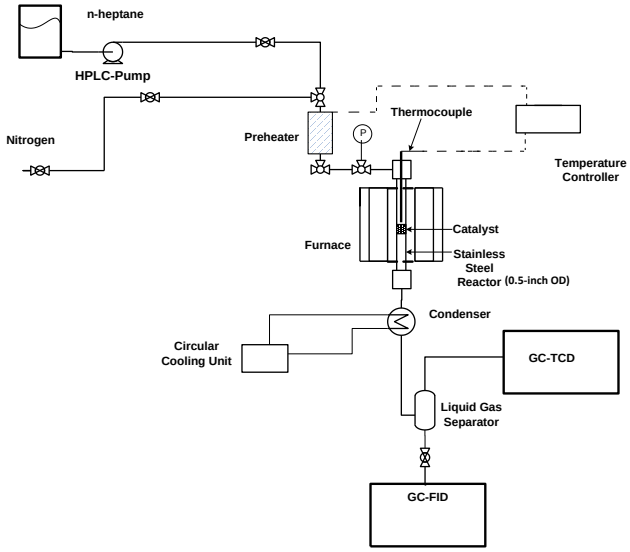

Figure 2 A fixed bed reactor system utilized in this research

3. RESULTS AND DISCUSSION

3.1 Catalysts characterization

Various methods were used to classify the synthesized zeolites. XRD analysis was used to analyze the composition of zeolites. Figure 5 displays the zeolites' XRD trends in the 2-theta radiation angle range and the 5–80° angle range after calcination. The index peaks for this sample in 2-theta are 7.78, 8.68, 23.09, 23.49, 23.77, and 24.29, which were detected in all catalysts ZSM-5 zeolite development before and after promoter processing, according to JCPDS results with reference code 00-037-0359 for ZSM-5 Zeolite. The XRD patterns of ZSM-5 and HZSM-5 showed peaks at 7–30° and 22.5–24°, representing the crystal plane of orthorhombic and monoclinic phase structure, respectively. The sharpness of the peaks shows the crystalline nature of the silicone samples. The findings indicate that during the impregnation phase, the promoters' crystallinity did not alter dramatically in the crystalline structure, mechanism change, or harm to the catalysts. The absence of any peaks linked to metal species means that the

promoter is distributed uniformly in the catalyst system [30, 31].

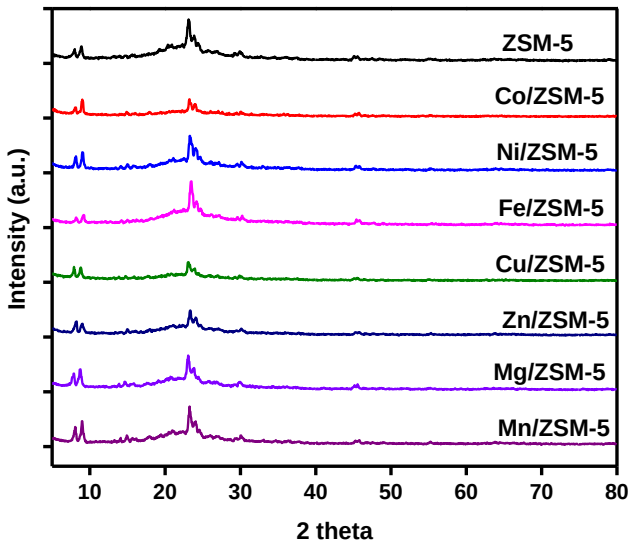

Figure 3 XRD pattern of zeolites

The Brunauer-Emmett-Teller (BET) method was employed to analyze all catalysts' textural properties, including surface area (S_{BET}), pore depth, and pore diameter. Table 2 displays the SBET surface area and total acidity (measured by TPR-NH_3) of ZSM-5, Fe/ZSM-5, Ni/ZSM-5, Co/ZSM-5, Cu/ZSM-5, Zn/ZSM-5, and Mn/ZSM-5 zeolites. Among the zeolites, the Zn/ZSM-5 exhibited a higher surface area, followed by Mn/ZSM-5. Nevertheless, in Fe/ZSM-5, the strong acidity needed for the isomerization reaction is high. The SBET was reduced from 413 to 284 m^2/g after loading 1wt% Fe on ZSM-5 due to heavy Fe contact with ZSM-5, suggesting that Fe was mainly deposited on the exterior surfaces could have prevented some of ZSM-5's micropores [32]. The S_{BET} reduced when 1 wt% Co, Ni, and Cu were introduced, but not as significant as when 1 wt% Fe was added. The drop in surface area of supported catalysts as compared to unpromoted catalysts may be attributed to the fact that certain metals, such as Fe, may increase the agglomeration of certain zeolite species, causing a drop in surface area [33].

Table 1 BET surface area, pore-volume, average pore diameter and acidity data of catalysts

Zeolites	**S_{BET} (m^2/g)**	**V_p (cm^3/g)**	**D_p (nm)**	**Acidity (m.mol NH_3/g)**
ZSM-5	413	0.38	3.68	0.37
Co/ZSM-5	308	0.45	5.84	0.42
Ni/ZSM-5	305	0.54	7.08	0.39
Fe/ZSM-5	284	0.48	6.76	0.53
Cu/ZSM-5	301	0.26	3.46	0.45
Zn/ZSM-6	378	0.44	4.66	0.41
Mn/ZSM-8	326	0.37	4.54	0.43

According to Gorzin et al. [31], the decreased surface area of promoted catalysts may be due to micropore damage or pore blockage. This result approves that partial structural damage may occur during the parent catalyst's impregnation; for example, the promoted samples lost some crystallinity, and the catalysts' crystal and particle sizes grew larger. The Zn/ZSM-5 catalyst behaved badly in terms of acidity, but it has a greater surface area than other promoted catalysts. As a result, it'll be important to see how low-acidity porosity affects the isomerization reaction.

FESEM imaging performed to investigate the morphology of catalysts in it is presented in Figure 4. FESEM micrographs of the catalysts show relatively uniform spherical aggregation. The pictures show that the support was an irregular particle and was made of porous sphere particles ranged from 16–38 nm. The promoted and pure ZSM-5 catalysts had identical surface morphologies and particle size distributions, suggesting no major morphology shift or structural disruption attributable to impregnation, which mirrored the XRD findings.

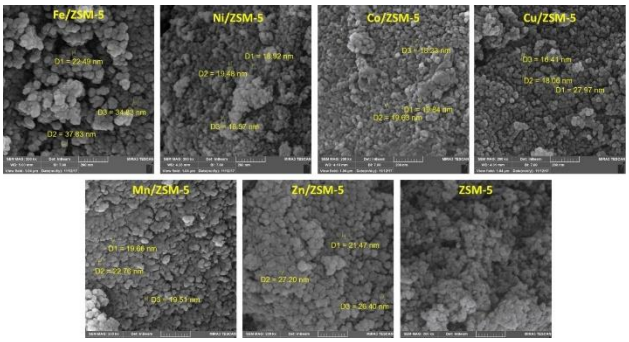

Figure 4 FESEM images of catalysts

The dispersion of metal in the zeolite support and promoters' impact on delivery were investigated using TEM on pure zeolite and the same catalysts. Results are shown in Figure . The products' high porosity is visible in the TEM, and these nano-sized characteristics are more readily noticed. ZSM-5 zeolites appeared to be hexagonal or spherical crystals with 1–5 m diameters and smooth surfaces, common in the ZSM-5 style [34-36]. The incorporation/deposition of the promoter molecules, depicted as dark-grey regions (10–30 nm), could be seen in the impregnated catalysts. In the impregnated samples, the incorporation/deposition of promoter particles may be seen as dark grey regions (10–30 nm). The TEM photos showed pale spots on mesoporous substrates' surfaces, which were traced to non-precious metal nanoparticles. On the other side, the metal nanoparticles were scattered in the help in a somewhat uneven fashion. As seen in the graphs, certain zeolite areas were heavily packed with metal particles, whilst others had just a few metal particles. The catalysts that have been promoted, as seen in TEM images of Fe/ZSM-5, Cu/ZSM-

5, and Mn/ZSM-5 a relatively better metal dispersion was observed.

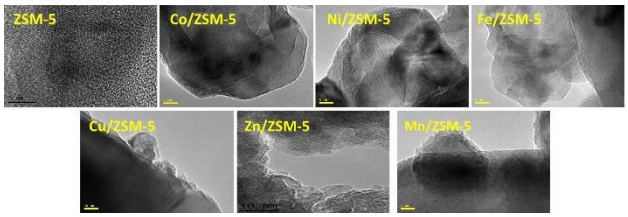

Figure 5 TEM images of zeolites

The reducibility of metals promoted ZSM-5 catalysts was investigated using H_2–TPR experiments. In Figure , the TPR curves for Fe/ZSM-5, Ni/ZSM-5, Co/ZSM-5, and Cu/ZSM-5 catalysts are displayed. The catalysts' TPR curves vary, suggesting an incompatible relationship between active phases [23, 24, 36, 37] and the difference in reducibility of the metal oxides in the zeolite.

In the temperature range tested, the H_2-TPR of pure ZSM-5 did not indicate hydrogen usage [38]. The prominent reduction peak at 462 °C corresponds to the Fe metal phase reduction. Ni and Co promoters' addition to ZSM-5 zeolite moved the H_2-TPR peaks to higher reduction temperatures, with the H2-TPR peak at 416 and 731 °C, respectively. That may be due to a more significant proportion of Ni and Co ions in the Ni and Co samples being completely depleted. With the Zn promoter in the ZSM-5, no major TPR peaks were observed. It was previously stated that the TPR profiles of zinc oxides are close to those of zinc-free iron oxides [39].

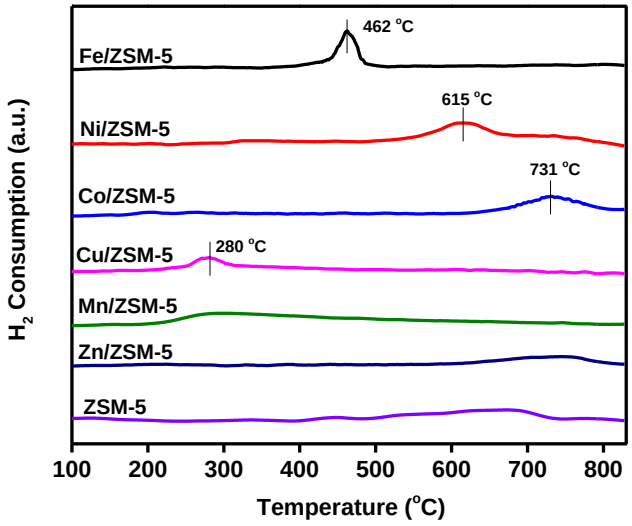

Figure 6 H_2-TPR profiles of the catalysts

3.2 Zeoforming reaction

The bifunctional catalysts, which consist of an acid function of ZSM-5 type zeolite and non-noble Fe, Mn, Ni, Co, Cu, and Zn metals function used for zeoforming reaction. The acidity of catalysts-controlled cyclization and isomerization reactions, while the metal function controlled the dehydrogenation and hydrogenation reactions. To achieve the best catalytic activity in zeoforming reactions, an appropriate equilibrium between such functions is essential. As shown in Table 3, the n-heptane conversion and catalytic activity of zeoforming have matched the acidity and surface area of catalysts. The catalyst's operation was assessed by converting n-heptane in a constant flow, a high-pressure micro-reactor system under reaction conditions of 400 °C and 10 bar pressures. The data from sulfur and n-heptane conversion and isomerization, octane number improvement, and the isomer composition were used to analyze the catalyst's activity. Sulfur was mixed as dimethyl disulfide (DMDS) at 1 wt% with n-heptane in the feed. The table shows that the increased yield from 12.22 wt.% (for pure ZSM-5) to 67.6 wt.% for the isomer when the Fe promoter impregnated.

Conversely, the cracked paraffin amount (C_1-C_6) decreased when the promoters applied for ZSM-5 zeolite. The product obtained for Fe/ZSM-5 catalyst appears to be reasonable for octane number enhancing (from 13 to 48.8) and zeoforming reaction. This reaction which increases 35.8 units in RON, could be used for blending of gasoline purpose. The Fe/ZSM-5 catalyst achieved the highest n-heptane conversion and sulfur portion, according to the results. The Fe/ZSM-5 catalyst's high activity is due to the addition of metal, which increases the acidity of the catalyst. It is also proved by previous studies, which revealed that the conversion of reactants is mainly determined by the acidity of the catalyst [40, 41].

There are few sequential reaction steps such as dehydrogenation (step 1), isomerization (step 2), and hydrogenation (step 3) for the isomerization reaction might involve. Reaction pressure could influence dehydrogenation and hydrogenation because these two reactions include various numbers of reactants to products. On this occasion, the low pressure enables the dehydrogenation reaction, and the high pressure allows the hydrogenation one. An intense observation of data given predicts that the reaction pressure slightly increased isoparaffin yields and the conversion. That may be attributed to the more successful conversion of iso-heptane olefin to hydrogenation in the third stage of the reaction relative to cracking. High n-heptane conversion (82.5 wt.%) and isoparaffin yield (73.05 wt.%) and 51.3 units for octane number were obtained at 20 bar; this is because the desorption and diffusion of molecules are more complex in high pressure.

The refining of hydrocarbons is followed by the deposition of carbonaceous deposits on the catalyst surface, a mechanism known as coking, which is the most common cause of catalyst deactivation. Deactivation happens in most catalytic processes and is affected by a combination of factors such as catalyst active site reactivity to foreign molecules such as sulfur and nitrogen compounds, alteration of reaction parameters, sintering (decrease in metallic, active surface area), and heavy metal deposition, which is

calculated at the end. In the last part of the experiment, time on stream behavior during n-heptane conversion was examined for the Fe/ZSM-5 at 10 bar pressures for 24 h, and the results are shown in Table . It can be seen that the feed conversion was decreased from 76.2% to 67.7% after 24 h of TOS. Catalyst selectivity, the yield of C6 crushed substance alkanes, and catalyst deactivation were both influenced by the solvent row's duration. In general, the Fe/ZSM-5 catalyst was selective for 1-hexene oligomerization due to the cracking reaction were blocked. The octane number also seems to be stable during 24 h of TOS (48.8-46.8).

During the zeoforming reaction, many reactions arise to transform n-heptane to paraffin, aromatic hydrocarbons, hydrogen sulfide, and sulfur-containing species to paraffin, aromatic hydrocarbons, and hydrogen sulfide. A simple reaction mechanism for the conversion of sulfur components in the zeoforming reaction is shown in Figure 7. The C–S bonds of mercaptans, sulfides, thiophenes, or their products are split, releasing hydrogen sulfide and olefin particles, as we discovered in previous studies [20]. The intermediate olefins are then transformed to paraffin and aromatics, while hydrogen sulfide, a gaseous C1–C4 species, is isolated along with side products of the whole phase.

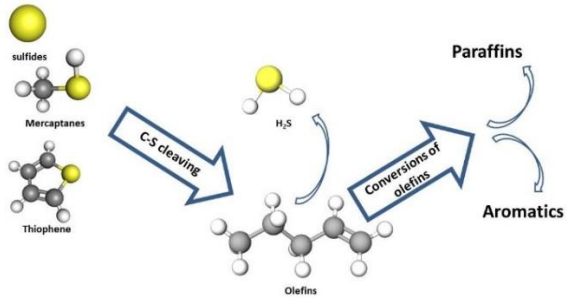

Figure 7 Proposed transform of sulfur-containing organisms in the zeoforming reaction

Table 2 Effect of promoters of ZSM-5 zeolite on zeoforming

Catalysts	**ZSM-5**	**Co/ZSM-5**	**Ni/ZSM-5**	**Fe/ZSM-5**	**Cu/ZSM-5**	**Zn/ZSM-5**	**Mg/ZSM-5**	**Mn/ZSM-5**
Conversion (wt %)	21.9	37.5	28.8	76.2	69.4	42.6	74.2	72.7
Gas yield (wt%)	5.8	4.5	7.9	15.3	5.1	14.3	3.6	3.6
Liquid yield (wt%)	94.2	95.5	92.1	84.7	94.9	85.7	96.4	96.4
Total Paraffins	86.86	69.17	80.44	28.92	37.33	67.49	31.17	34.47
(i)Cracked Paraffins (C1-C6)	3.3	4.9	7.9	9.3	6.1	5.38	8.6	7.6
(ii) n-heptane	83.56	64.27	72.54	19.62	31.23	62.11	22.57	26.87
Total i-Paraffins	12.22	26.31	17.58	67.6	61	31.52	65.73	62
(i)Lower i-paraffins (iC4-iC6)	3.8	5.31	5	9.6	9.4	7.9	9.6	7.7
(ii) C7+ i-paraffins	8.42	21	12.58	58	51.6	23.62	56.13	54.3
a) Mono-branched	7.4	18.2	11.3	43.4	41.1	19.6	43.1	42.4
b) Di-branched	1.02	2.8	1.28	13.1	10.4	4	12.43	11.4
c) Multi-branched	0	0	0	1.5	0.1	0.02	0.6	0.5
Olefins	0	1.2	0.1	0.1	0.1	0	0	0.1
Naphthenes	0	2.3	1	2.4	0.7	0	2.2	2.5
Aromatics	0	0.4	0.2	0.9	0.6	0.6	0.8	0.8
Sulfur	0.92	0.62	0.68	0.08	0.27	0.39	0.1	0.13
Total	100	100	100	100	100	100	100	100
RON	13	25.5	16.4	48.8	45.5	35.2	47.5	47.5

Table 3 Effect of pressure on zeoforming reaction

Pressure (bar)	10	15	20	25
Conversion (wt %)	76.2	78.3	81.9	82.5
Gas yield (wt%)	15.3	12.8	12.8	14.1
Liquid yield (wt%)	84.7	87.2	87.2	85.9
Total Paraffins	28.92	25.76	25.32	23.04
(i)Cracked Paraffins (C1-C6)	9.3	4.1	4.1	4
(ii) n-heptane	19.62	21.66	21.22	19.04
Total i-Paraffins	67.6	70.6	71.4	73.05
(i)Lower i-paraffins (iC4- iC6)	9.6	8.4	7.5	6.6
(ii) C7+ i-paraffins	58	62.2	63.9	66.45
a) Mono-branched	43.4	46.8	46.8	47.2
b) Di-branched	13.1	13.9	15.4	17.5
c) Multi-branched	1.5	1.5	1.7	1.75
Olefins	0.1	0.1	0	0.1
Naphthenes	2.4	2.5	2.2	2.7
Aromatics	0.9	0.98	1.05	1.1
Sulfur	0.08	0.06	0.03	0.01
Total	100	100	100	100
RON	48.8	49.5	49.8	51.3

Table 4 Time on stream for Fe/ZSM-5

Time (h)	1	4	8	12	16	20	24
Conversion (wt %)	76.2	74.8	69.3	68.7	67.8	67.9	67.7
Gas yield (wt%)	15.3	14.9	14.1	15.1	14.3	14.1	14.6
Liquid yield (wt%)	84.7	85.1	85.9	84.9	85.7	85.9	85.4
Total Paraffins	28.92	29.1	29.2	29.7	29.8	29.8	29.8
(i)Cracked Paraffins (C1-C6)	9.3	9.2	9.1	8.9	8.9	8.7	8.6
(ii) n-heptane	19.62	19.9	20.1	20.8	20.9	21.1	21.2
Total i-Paraffins	67.6	67.44	67.32	67.14	67.04	67.27	67.46
(i)Lower i-paraffins (iC4- iC6)	9.6	9.74	10.32	9.74	9.34	11.97	12.96
(ii) C7+ i-paraffins	58	57.7	57	57.4	57.7	55.3	54.5
a) Mono-branched	43.4	43.1	42.9	43.5	44.1	42.1	41.8
b) Di-branched	13.1	13.1	12.9	12.8	12.7	12.5	12.1
c) Multi-branched	1.5	1.5	1.2	1.1	0.9	0.7	0.6
Olefins	0.1	0.1	0.2	0.1	0.3	0.1	0.1
Naphthenes	2.4	2.4	2.3	2.1	1.9	1.9	1.7
Aromatics	0.9	0.87	0.87	0.85	0.84	0.81	0.81
Sulfur	0.08	0.09	0.11	0.11	0.12	0.12	0.13
Total	100	100	100	100	100	100	100
RON	48.8	47.5	47.2	47.1	46.9	46.8	46.8

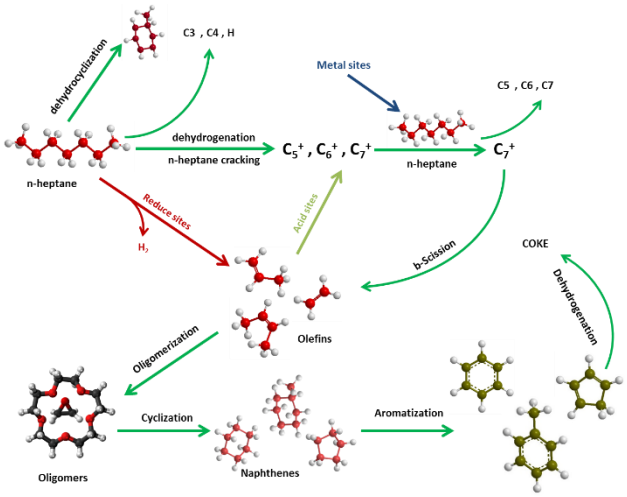

Figure 8 Proposed zeoforming reaction pathway

4. CONCLUSION

One of the essential processes in the processing industry is catalytic naphtha reforming. This system is generally used to make high-octane gasoline and aromatic materials. However, there are drawbacks in this technology such as sulfur emission, employing high costs units such as hydrodesulfurization (HDS) process, and high costs of catalysts. In this work, the bibliometric analysis found that conversion, performance, hydrocarbons, zsm-5, and zeolite have the highest total link strength and top occurrences by using keywords such as “naphtha” and “zeolite” search in the WOS database. In contrast, there is a lack of research in the title search of keywords such as “zeoforming” and “hydrodesulfurization” from 1970 to 2021. It is anticipated that scientists would be motivated to use and adapt these seeking methods and techniques to their study due to understanding that specific knowledge is right at their fingertips. Thus we carried out the zeoforming process using n-heptane as a model compound of naphtha over pure ZSM-5 type zeolite and promoted ZSM-5 such as Fe/ZSM-5, Ni/ZSM-5, Co/ZSM-5, Cu/ZSM-5, Zn/ZSM-5, and Mn/ZSM-5 zeolitic catalysts and examined their catalytic activities for zeoforming reaction and to produce high octane of mixed feedstocks such as naphtha. XRD, H_2-TPR, BET, TEM, and FESEM analyses enable the characterization of catalysts to elucidate the performance's reasonable compared to unpromoted ZSM-5 by showing non-noble metal ability to promote metal dispersion, catalyst crystallinity and provide the catalyst with the suitable acidity to enhance the octane number. The present study exemplified that the acid sites considerations for Fe/ZSM-5 catalyst play a vital role in the effective isomerization and octane number boosting. The catalyst can be economically viable in industrial applications. The addition of non-noble metals to the ZSM-5 helps increases both n-heptane conversion and aromatic selectivity. It may be due to the Fe promoter's existence raising the catalyst's dehydrogenation activity, resulting in higher availability of the olefin pool, which is the intermediate for aromatization. This indicates that Fe species are capable of dehydrating intermediates and turning them into aromatics.

ACKNOWLEDGEMENTS

The principal author, Walid Nabgan, is thankful for Universiti Teknologi Malaysia's support in the form of the Post-Doctoral Fellowship Scheme "Simultaneous heavy metals ions and organic pollutants photoredox reactions over SiO_2/ZrO_2 based catalysts under solar-light irradiation" (PDRU Grant number: 05E49). In addition, the authors acknowledge the financial support given for this work by Universiti Teknologi Malaysia (UTM) under the Collaborative Research Grant (CRG) number 07G61 and the University Laboratory Management Unit (UPMU).

REFERENCES

[1] Sharifi K, Halladj R, Royaee SJ, Nasr MRJ. Powder Technology. 2018;338:638-44.
[2] Klimov OV, Koryakina GI, Gerasimov EY, Dik PP, Leonova KA, Budukva SV, et al. Catalysis in Industry. 2015;7:38-46.
[3] Hein J, Gutierrez OY, Schachtl E, Xu PH, Browning ND, Jentys A, et al. ChemCatChem. 2015;7:3692-704.
[4] Huirache-Acuña R, Alonso-Núñez G, Paraguay-Delgado F, Lara-Romero J, Berhault G, Rivera-Muñoz EM. Catalysis Today. 2015;250:28-37.
[5] Klimov OV, Nadeina KA, Dik PP, Koryakina GI, Pereyma VY, Kazakov MO, et al. Catalysis Today. 2016;271:56-63.
[6] Liu YJ, Song SZ, Deng X, Huang W. Energy & Fuels. 2017;31:7372-81.
[7] Nikulshina MS, Mozhaev AV, Minaev PP, Fournier M, Lancelot C, Blanchard P, et al. Russian Journal of Applied Chemistry. 2017;90:1122-9.
[8] Boldushevskii RE, Guseva AI, Vinogradova NY, Naranov ER, Maksimov AL, Nikul'shin PA. Russian Journal of Applied Chemistry. 2018;91:2046-51.
[9] Dik PP, Pereima VY, Nadeina KA, Kazakov MO, Klimov OV, Gerasimov EY, et al. Catalysis in Industry. 2018;10:20-8.
[10] Behnejad B, Abdouss M, Tavasoli A. Petroleum Science. 2019;16:645-56.
[11] Valdes-Martinez OU, Santolalla-Vargas CE, Santes V, de los Reyes JA, Pawelec B, Fierro JLG. Catalysis Today. 2019;329:149-55.
[12] Abubakar UC, Alhooshani KR, Adamu S, Al Thagfi J, Saleh TA. Journal of Cleaner Production. 2019;211:1567-75.
[13] Villasana Y, Mendez FJ, Luis-Luis M, Brito JL. Fuel. 2019;235:577-88.
[14] Blanco-Brieva G, Campos-Martin J, Al-Zahrani S, Fierro J. Removal of refractory organic sulfur compounds in fossil fuels using MOF sorbents. Global Nest J. 2010;12:296-304.
[15] Zhao N, Li S, Wang J, Zhang R, Gao R, Zhao J, et al. Journal of Solid State Chemistry. 2015;225:347-53.
[16] Duan AJ, Li TS, Niu H, Yang X, Wang ZG, Zhao Z, et al. Catalysis Today. 2015;245:163-71.
[17] Harrhy JH, Wang A, Jarvis JS, He P, Meng S, Yung M, et al. Communications Chemistry. 2019;2:37.
[18] Yin C, Liu C. T, Petroleum Science and Technology. 2005;23:1153-6
[19] Yin C, Liu C. Applied Catalysis A: General. 2004;273:177-84.
[20] Nabgan W, Rashidzadeh M, Nabgan B. Environmental Chemistry Letters. 2018;16: 507–22..

[21] Soltanali S, Halladj R, Rashidi A, Bazmi M, Bahadoran F. Chemical Engineering Research and Design. 2016;106:33-42.
[22] Soltanali S, Halladj R, Rashidi A, Bazmi M. Crystal Research and Technology. 2014;49:366-75.
[23] Nabgan W, Tuan Abdullah TA, Mat R, Nabgan B, Gambo Y, Triwahyono S. International Journal of Hydrogen Energy. 2016; 41:22922-31.
[24] Nabgan W, Tuan Abdullah TA, Mat R, Nabgan B, Gambo Y, Moghadamian K. Journal of Environmental Chemical Engineering. 2016; 4:2765-73.
[25] Andrigo P, Bagatin R, Pagani G.. Catalysis Today. 1999; 52:197-221.
[26] Eigenberger G, Ruppel W. Ullmann's Encyclopedia of Industrial Chemistry: Wiley-VCH Verlag GmbH & Co. KGaA; 2000.
[27] Beltramini JN, Fang R. Studies in Surface Science and Catalysis. 1996; 100:465-75.
[28] Balaban A, Kier L, Joshi N. MATCH Commun Math Comput Chem. 1992; 28:13-27.
[29] Hasan M, Mohamed AM, Al-Kandari H. Molecular Catalysis. 2018;452:1-10
[30] Rostamizadeh M, Jalali H, Naeimzadeh F, Gharibian S. Physical Chemistry Research. 2019; 7:37-52.
[31] Gorzin F, Yaripour F. Research on Chemical Intermediates. 2019; 45:261-85.
[32] Kostyniuk A, Key D, Mdleleni M. Journal of Saudi Chemical Society. 2019; 23:612-26.
[33] Uykun Mangaloğlu D, Baranak M, Ataç Ö, Atakül H. Journal of Industrial and Engineering Chemistry. 2018; 66:298-310.
[34] Cheng K, Zhang L, Kang J, Peng X, Zhang Q, Wang Y. Chemistry – A European Journal. 2015; 21:1928-37.
[35] Moon S, Chae H-J, Park MB. Applied Catalysis A: General. 2018; 553:15-23.
[36] Nabgan W, Abdullah TAT, Mat R, Nabgan B, Jalil AA, Firmansyah L, et al. International Journal of Hydrogen Energy. 2017; 42:8975-85.
[37] Nabgan W, Tuan Abdullah TA, Mat R, Nabgan B, Triwahyono S, Ripin A. Applied Catalysis A: General. 2016; 527:161-70.
[38] Van der Borght K, Galvita VV, Marin GB. Applied Catalysis A: General. 2015; 492:117-26.
[39] Denardin F, Perez-Lopez OW. Fuel. 2019; 236:1293-300.
[40] Zhang X, Cheng D-g, Chen F, Zhan X. Chemical Engineering Science. 2017; 168:352-9
[41] Xu S, Zhang X, Cheng D-g, Chen F, Ren X. Frontiers of Chemical Science and Engineering. 2018; 12:780-9.
[42] Asaftei IV, Lungu NC, Sandu IG, Spac AF, Ignat M. Revista De Chimie. 2018; 69:2420-4.

Malaysian Journal of Catalysis
http://mjcat.utm.my/
MJCat
Research Article

Effect of Calcination Temperature On Structure of Silica Doped On Zirconia for Photodegradation of 2-Chlorophenol

N.S. Hassan[a*], A.A. Jalil[a,b] and M.H. Sawal[a]

[a]*School of Chemical and Energy Engineering Engineering, Faculty of Engineering, Universiti Teknologi Malaysia, 81310 UTM Johor Bahru, Johor, Malaysia*
[b]*Centre of Hydrogen Energy, Institute of Future Energy, 81310 UTM Johor Bahru, Johor, Malaysia*

**Corresponding Author: nurulsahida@utm.my*

Article history :
Received 21 September 2021
Accepted 4 October 2021

GRAPHICAL ABSTRACT

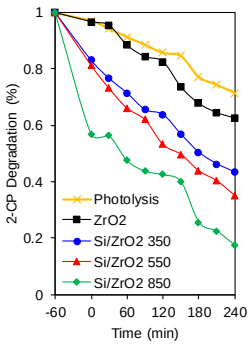

ABSTRACT

Simple microwave assisted method was employed to prepare silica (SiO_2) doped zirconia (ZrO_2) that synthesized under different calcination temperature which are 350, 550 and 850 °C and denoted as Si/ZrO_2-350, Si/ZrO_2-550 and Si/ZrO_2-850, respectively for photodegradation of 2-chlorophenol (2-CP). The synthesized catalysts were characterized by X-ray diffraction, Fourier transform infrared and ultraviolet-visible diffuse reflectance spectroscopy. The results showed that higher calcination temperature and the presence of Si induced the tetragonal phase of ZrO_2 as well as narrowed the band gap energy, which affected the photocatalytic activity. The catalyst was subsequently tested for the photocatalytic activity on 2-CP degradation under various parameters such as pH, catalyst dosage and initial concentration of 2-CP under visible light irradiation. Si/ZrO_2-850 showed the highest photodegradation of 2-CP due to presence of tetragonal phase on ZrO_2 that resulting stabilize the structure. The photocatalytic performance of the catalysts towards degradation of 10 mgL^{-1} of 2-CP at pH 3 and 0.125 g L^{-1} catalyst under visible light after 240 minutes as following order: Si/ZrO_2-850 (88%) > Si/ZrO_2-550 (65%) > Si/ZrO_2- 350 (57%) > ZrO_2-850 (37%). The photodegradation followed the pseudofirst order Langmuir-Hinshelwood kinetic model. This study demonstrated that the Si/ZrO_2 has a potential to be used in photocatalytic degradation of various organic pollutant.

Keywords: Calcination temperature; Microwave; Silica-zirconia; 2-chlorophenol

| eISSN 0128-2581 |

1. INTRODUCTION

2-chlorophenol (2-CP) is a common organic compound found in wastewater as it is introduced mainly by chemical and pharmaceutical industry. It has been widely used as an antiseptic, as manufacture of insecticide profenofos and as an organic synthesis dye. Numerous industries have utilized 2-CP as intermediated chemical [1]. However, this intermediate is very risky in the situation of skin exposure (irritant), swallowing, inhalation and in the condition of eye contact (irritant). Excessive over-exposure will contribute to the death [2]. The resilience of the C-Cl bond in halo hydrocarbons is responsible for its toxicity and consistency in the biological system [3]. Hence, degradation of 2-CP into harmless product should be discovered rapidly before many people can get infected.

Nowadays, advanced oxidation processes (AOPs) have gained much attention as a promising method that can effectively degrade the organic pollutant in the wastewater [4,5]. This approach is characterized as oxidation processes involving the in-situ production of powerful oxidizing agents such as hydroxyl radicals (•OH) at appropriate concentrations to effectively decontaminate wastewater [6,7]. AOPs concept has been enlarge nowadays such as oxidative processes with sulfate radicals [8]. The effectiveness of AOPs will be decided by the production of reactive free radicals predominantly •OH.

Photocatalysis is one of the methods that employed from the AOPs. Zirconia (ZrO_2), one of the most suitable semiconductor photocatalysts, was widely used to degrade of organic pollutants [9]. However, the photocatalytic efciency of ZrO_2 is constrained by three key drawbacks [10, 11]. First, the small spectral response interval limits the UV region absorption range, which only accounts for less than 5% of the entire solar range. Then, the high electron–hole recombination rate results in low quantum yield. In addition, tetragonal phase (*t*-ZrO_2) stabilization typically involves

higher temperatures (> 1000 °C) and/or suitable dopants with different valency, size, and electronegativity characteristics. Therefore, several eforts have been done to stabilize its phase and improve the photocatalytic efciency of ZrO_2 as well as application potential of ZrO_2 [12]. Besides, altering the catalyst's physicochemical properties also enhanced the photocatalytic activity, mainly via calcination temperature [13]. Thus, in this study, synthesis of ZrO_2 by doping with SiO_2 will be focused on varying the calcination temperature that could increase the effectiveness of photodegradation of 2-CP. The ZrO_2 and SiO_2/ZrO_2 was synthesized by using microwave-assisted method and calcined under different calcination temperature (350, 550 and 850°C). The physicochemical properties of Si/ZrO_2 was analyzed by using X-ray diffraction, Fourier transform infrared and ultraviolet-visible diffuse reflectance spectroscopy. Photocatalytic activity of the photocatalysts was conducted under various parameters such effect of pH (3-11), catalyst dosage (0.125-0.625 g L^{-1}) and initial 2-CP concentration (10-100 mg L^{-1}).

2. EXPERIMENTS

2.1 Materials

2-CP, cetyltrimethylammonium bromide (CTAB), 2-propanol (Pr-OH), zirconium (IV) propoxide (ZrP), (3-aminopropyl)triethoxysilane (APTES) and ammonium hydroxide solution (NH_4OH) were purchased from Sigma Aldrich. Other than that, the all reagents were prepared using deionized water.

2.2 Catalyst Preparation

The Si/ZrO_2 was synthesized by using microwaveassisted method. Firstly, 4.8 g of CTAB surfactant was dissolved in the solution which is contained with 720 mL distilled water, 29 mL of 8 M NH_4OH and 120 mL propanol. The mixture then was stirred continuously for 30 min at 50 °C. 5.7 mL of ZrP was added into the mixture followed by 1.053 mL of APTES and stirred for 2 hours. The white solution was heated by using the microwave under a frequency of 2.45 GHz and heating power of 450W for 2 hours. The final product was dried overnight in oven before calcined at 850 °C for 3 hours and denoted as Si/ZrO_2-850. Similar procedure was applied for various calcination temperature of 350˚C, 550˚C and 850˚C and denoted as Si/ZrO_2-350, Si/ZrO_2-550 and Si/ZrO_2-850, respectively.

2.3 Characterization

The catalysts crystallinity were verified by D8 ADVANCE Bruker X-ray diffractometer. Meanwhile, Meanwhile, the chemical properties of the catalysts were detected by the KBr method via Perkin Elmer Spectrum GX FT-IR. The optical properties of the catalyst were measured by using Agilent Technologies Cary 60 UV-Vis spectrometer.

2.4 Catalytic testing

The photodegradation of 2-CP was carried out in a batch reactor, which fixed with cooling system, employing 400 W metal halide lamps. Before 0.375 g L^{-1} catalyst in 100 mL 2-CP solution (10 mg L^{-1}) being exposed to light radiation, the catalyst was stirred at pH = 5 in the dark for 1 h to achieve the equilibrium of adsorption/desorption. Each series of experiment was performed three times to ensure the consistency.

3. RESULTS AND DISCUSSION

Figure 1 shows a wide angle of XRD diffractogram of the commercial ZrO_2 and synthesized of Si/ZrO_2 under different calcination temperatures (350 °C, 550 ºC and 850 °C). The Si/ZrO_2-350 only showed the existence of the monoclinic phase (*m*-ZrO_2) with XRD peak at 2θ= 22° and 28.1º (ICDD No-01-083-0944) [14]. The Si/ZrO_2 synthesized catalysts is well indexed to *t*-ZrO_2 (ICDD No-01-079-1765) with the prominent XRD at 29.9° (101), 34.8° (110), 50.1° (112) and 60.0° (211) [15] when the calcination temperature increases up to 550 ºC. Interestingly, increased up to 850 ºC, the catalyst possessed the higher *t*-ZrO_2 phase without any phase impurities evidently confirmed by presence of additional peaks at 2θ= 34.8º (200), 50.1º (220) and 59.9º (311). In fact, the tetragonal crystalline form of ZrO_2 is most commonly used in catalysis and related activities and is therefore a technologically significant product. Both *t*-ZrO_2 and *m*-ZrO_2 were observed for commercial ZrO_2. This result shows that the presence of Si and higher calcination temperature could stabilize the *t*-ZrO_2.

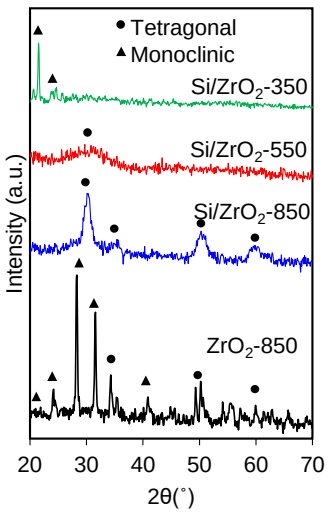

Figure 1: XRD patterns of all catalysts

For chemical properties studies, all the catalysts were then characterized by FTIR and the spectra in the region of 4000-400 cm^{-1} are shown in Figure 2. The Si/ZrO2 catalysts showed five main bands, which attributed to hydroxyl stretching (–OH, 3456 cm^{-1}), –OH vibration of the surface-adsorbed water (1620 cm^{-1}), Zr–OH bond (1384 cm^{-1}), Si–O–Si asymmetric stretching (1070 cm^{-1}), and t-ZrO_2 (464 cm^{-1}) [16,17]. The band at 740 cm^{-1} was observed only for Si/ZrO_2-350 and Si/ZrO_2-550, which correspond to the *m*-ZrO_2. Similarly, these phase also was observed for ZrO_2-850. As seen, the band at 1384 cm^{-1} was disappeared for Si/ZrO_2-550 and Si/ZrO_2-850, suggesting that the higher of calcination temperature could dispersed the Si well on the surface of ZrO_2 and the Si species may interact with ZrO_2 [16, 18]. Among all Si/ZrO_2 catalyst, Si/ZrO_2-850 showed the higher intensity of the band at 464 cm^{-1}, indicated that this catalyst possessed higher *t*-ZrO_2 which in line with XRD analysis.

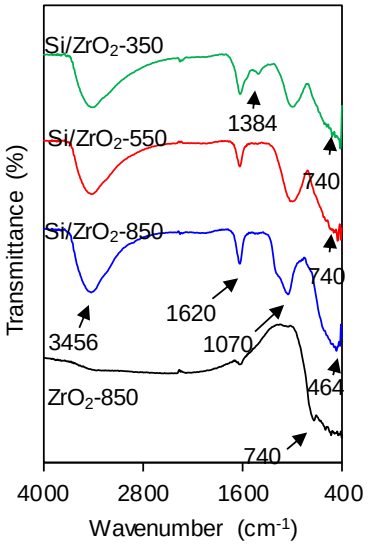

Figure 2: FTIR spectra of all catalysts

Band gap of the photocatalysts play an important key role in photocatalytic applications. The catalysts were then subjected to UV-Vis DRS to analyse band gap energy. Figure 3 illustrates the wavelength measurement to calculate bandgap energy. The bandgap of the samples was calculated using the equation of E = 1240/λ, where E is the band gap energy in eV and λ is the wavelength in nanometres [19]. The summary of the band gap for all catalysts are stated in Table 1. Si/ZrO_2-850 showed the lowest band gap energy (2.64 eV) compared to commercial ZrO_2 (4.35 eV). The reduction of bandgap after Si doped on ZrO_2 at higher temperature is might be due to the more formation of surface defect [3]. While, among all synthesized Si/ZrO_2, Si/ZrO_2-850 showed the lowest band gap energy and this result led to the potential use of it in visible light responsive photocatalytic reaction.

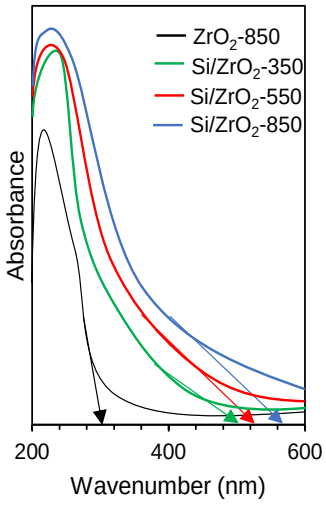

Figure 3: UV-Vis DRS for all catalysts

Table 1 Band gap of the catalysts

Catalyst	Band Gap (eV)
ZrO_2-850	4.35
Si/ZrO_2-350	2.33
Si/ZrO_2-550	2.29
Si/ZrO_2-850	2.21

The photocatalytic performance of the synthesized catalysts was evaluated on photodegradation of 2- CP and the results are shown in Figure 4 under visible light irradiation for 240 minutes. The photolysis of 2-CP shows only 30% of 2-CP is degraded, indicating the pollutant's higher stability. The 2-CP degradation was activated by electronically excited 2-CP via direct light absorption, resulting in cleavage of the C–CI bond. Si/ZrO_2-850 (83%) catalyst was exhibited the highest photocatalytic performance compared to the Si/ZrO_2-550 (65%), Si/ZrO_2-350 (57%) and ZrO_2-850 (37%). This is due to higher of tetragonal phase of zirconia and narrowing of its band gap which can led to decrease in electron-hole recombination rate [20,21].

In fact, the optimum pH was found to be 3 after varying the pH from 3 to 11 (Figure 5A). This result may be explained by the amphoteric behavior of the catalyst when the photoreaction takes place on its surface, which is dependent on the basis of the zero-pointcharge (pH_{ZPC}). The inset figure shows that the pH_{ZPC} was found to be at pH 6. Indeed, the catalyst surface would be positively charged below this pH value and electrostatically attracted to the negatively charged of 2-CP, and vice versa [16,18]. Thus, the optimum reaction conditions are in acidic conditions.

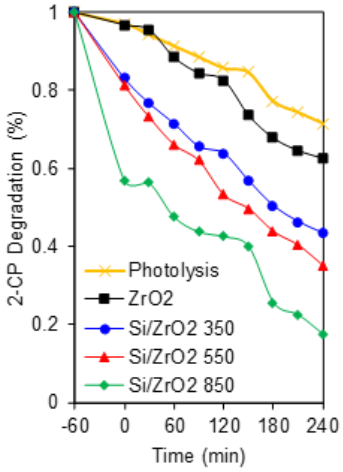

Figure 4: Photodegradation of 2-CP using different type of catalyst ([2-CP] = 10 mgL^{-1}, W= 0.375 g L^{-1}, pH=3).

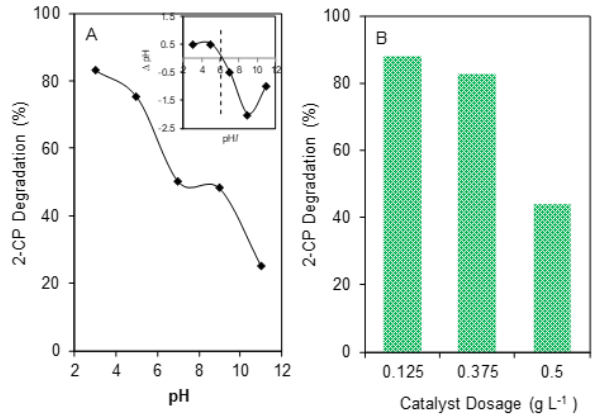

Figure 5: Effect of (A) pH and (B) catalyst dosage towards photodegradation of 2-CP using Si/ZrO_2-850

While the optimum catalyst dosage was 0.375 g L^{-1} to give 83% degradation of 2-CP, due to after the optimum catalyst loading is accomplished (Figure 5B). This is because the higher the catalyst dose, the higher the number of active sites that could absorb more photons and 2-CP. However, excess catalytic dosage may create greater turbidity, which would reduce its penetration because of light dispersed and inhibit the photocatalytic mechanism [18,22]. Nevertheless, the number of active sites and the formation of reactive oxygen species (ROS) will increase correspondingly when the amount of catalyst dosage increased [23]. Adequate loading of the catalyst enhances the efficiency of generation of electron/hole pairs to boost the degradation of pollutants [2,3].

The initial concentration of 2-CP is one of the driving parameters in photodegradation of 2-CP. The effect of the initial concentration on 2-CP degradation was studied by preparing different number of 2-CP solutions (10-100 mgL^{-1}). Figure 6A shows that the photocatalytic activity was decreased with increasing the initial concentration of 2-CP over constant catalyst dosage. This reaction was favourable at low concentration which is 10 mg L^{-1}. In fact, the penetration of light to the surface of the catalyst has been hampered, most likely due to the deposition of contaminants covering the surface of the catalyst [4,18].

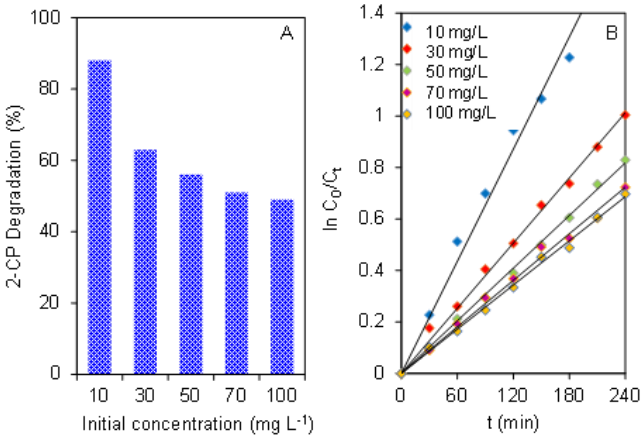

Figure 6: (A) Photodegradation of 2-CP with different initial concentrations of 2-CP and (B) Photodegradation kinetics of 2-CP using Si/ZrO_2-850 at different initial concentrations (W=0.125 g L^{-1}, pH= 3).

In general, the kinetics of most organic compounds undergoing photocatalytic reactions are defined in a pseudo first-order model, which is rationalised in terms of the Langmuir-Hinshelwood model modified to accommodate reactions that have occurred at the solid-liquid interface [24]. At low initial 2-CP concentration, the simplest equation for the rates of photodegradation of 2-CP is given by the equation 1 and 2 [24].

$$\ln C_t = -kt + \ln C_0 \quad (1)$$

where k is the pseudo first-order rate while C_o and C_t are the concentrations of 2-CP initially and at time t, respectively. The integration of (Equation 1) yields the (Equation 2),

$$\ln\left(\frac{C_o}{C_t}\right) = k_r K t = k_{app} t \quad (2)$$

The linearity of the ln (C_0/C_t) plot vs. the irradiation time shown in Figure 6B confirmed that the reaction process implemented the pseudo-first order kinetics model. Line slope was the apparent first-order rate constant (k_{app}) and the value obtained (Table 2) showed an important and beneficial

Table 2 Percentage degradation at different initial concentration of PCT and pseudo-first-order apparent constant values for PCT degradation using 5% Fe_3O_4/WTC [W= 0.4 g/L, t=2 h, pH=5, T= 30°C].

Initial concentration of 2-CP, C_o (mg L^{-1})	Degradation (%)	Reaction rate, k_{app} (x 10^{-2} mg L^{-1} min^{-1})	Initial rate, r_o (x 10^{-1} mg L^{-1} min^{-1})
10	83	7.30	7.3
30	63	4.20	12.6
50	56	3.40	17.0
70	51	0.30	21.0
100	49	0.29	29.0

effect of the Si/ZrO_2-850 on the photodegradation of the 2-CP. The k_{app} values decreased with an increasing initial concentration, suggesting that the system is favourable at a low concentration [25]. At a lower concentration, the reaction rate is able to manage the mechanism, since the active sites on the catalyst's surface were only partly occupied by adsorbed 2-CP molecules. As a result, at higher concentrations, hydroxyl radicals become a restricting reactant and thus lower the reaction rate**.**

The line with an intercept of $1/k_r$ and $1/k_rK_{LH}$ was obtained from the Langmuir Hinshelwood (L-H) kinetic formula (Equation 3) [6],

$$\frac{1}{r_o} = \left[\frac{1}{k_r K_{LH}}\right]\left[\frac{1}{C_o}\right] + \frac{1}{k_r} \qquad (3)$$

where k_r is the reaction rate constant (mg L^{-1} min^{-1}), K_{LH} is the adsorption coefficient of the reactant (L mg^{-1}) and C_o is the initial concentration of 2-CP (mg L^{-1}). The calculated values of k_r and K_{LH} were 0.012 mg L^{-1} min^{-1} and 0.003 L mg^{-1}, respectively. These results illustrated that since k_r, > K_{LH}, suggesting that 2-CP adsorption on the surface of Si/ZrO_2- 850 was controlling step in the photodegradation [6].

4. CONCLUSION

In this study, silica loaded on zirconia (Si/ZrO_2) was successfully synthesized by microwave-assisted method under various calcination temperature, which were then characterized by XRD, FTIR and UV-Vis/DRS. The results showed that higher calcination temperature and the presence of Si induced the tetragonal phase of ZrO_2 as well as narrowed the band gap energy, which affected the photocatalytic activity. The photocatalytic performance of the catalysts towards degradation of 10 mg L^{-1} of 2-CP at pH 3 and 0.125 g L^{-1} catalyst for 240 minutes under visible light was in the following order: Si/ZrO_2-850 (88%) > Si/ZrO_2-550 (65%), Si/ZrO_2-350 (57%) > ZrO_2-850 (37%). Si/ZrO_2-850 shows the highest photocatalytic performance due to narrow band gap, high crystallinity and more tetragonal phase.

ACKNOWLEDGEMENTS

The authors are grateful for the financial support by the Universiti Teknologi Malaysia through Professional Development Research University Grant (No. 05E44).

REFERENCES

[1] M.S. Azami, A.A. Jalil, C.N.C. Hitam, N.S. Hassan, C.R. Mamat, R.H. Adnan, N. Chanlek, Appl. Surf. Sci. 512 (2020) 145744.
[2] A.A. Fauzi, A.A. Jalil, C.N.C. Hitam, F.F.A. Aziz, N. Chanlek, J. Environ. Chem. Eng. 8 (2020) 104484.
[3] N.S. Hassan, A.A. Jalil, F.F.A. Aziz, A.A. Fauzi, M.S. Azami, N.W.C. Jusoh, Top. Catal. 63 (2020) 1145–1156.
[4] N.F. Khusnun, A.A. Jalil, S. Triwahyono, N.W.C. Jusoh, A. Johari, K. Kidam, Phys Chem Chem Phys 18 (2016) 12323–12331
[5] C.N.C. Hitam, A.A. Jalil, Y.O. Raji, Top Catal. 63 (2020) 1169-1181.
[6] A.F.A. Rahman, A.A. Jalil, S. Triwahyono, A. Ripin, F.F.A. Aziz, N.A.A. Fatah, N.S. Hassan, J. Clean. Prod. 143 (2017) 948-959.
[7] F.H. Mustapha, A.A. Jalil, Mohamed M, S. Triwahyono, N.S. Hassan, N.F. Khusnun, A.S. Zolkifli, J. Clean. Prod. 168 (2017) 1150–1162.
[8] A.A. Fauzi, A.A. Jalil, N.S. Hassan, F.F.A. Aziz, M.S. Azami, I. Hussain, D.V. Vo, Chemosphere (2021) 131651.
[9] F.F.A. Aziz, A.A. Jalil, N.F. Khusnun, C.N.C. Hitam, A.F.A. Rahman, A.A. Fauzi, J. Hazard. Mater. 401 (2020) 123277.
[10] N.S. Hassan, A.A. Jalil, N.F. Khusnun, M.W. Ali, S. Haron, J. Alloys. Compd. 78 (2019) 221–230.
[11] M.V. Carevic, N.D. Abazovic, T.B. Novakovic, V.B. Pavlovic, M.I. Comor, Appl. Catal. B. 195 (2016) 112–120.
[12] A.U. Maheswari, S.S. Kumar, M. Sivakumar, Ceram. Int. 40 (2014) 6561–6568.
[13] A. Kumar, M. Naushad, A. Rana, G. Sharma, A.A. Ghfar, F.J. Stadler, M.R. Khan, Int. J. Biol. Macromol. 104 (2017) 1172–1184.
[14] J. Zhang, Y. Gao, X. Jia, J. Wang, Z. Chen, Y. Xu, Sol. Energy Mater. Sol. Cells. 182 (2018) 113–120
[15] R. Dwivedi, A. Maurya, A. Verma, R. Prasad, K.S. Bartwal, J. Alloys Compd. 509 (2011) 6848–6851.
[16] N.S. Hassan, A.A. Jalil, S. Triwahyono, C.N.C. Hitam, A.F.A. Rahman, N.F. Khusnun, D. Prasetyoko, J. Taiwan. Inst. Chem. Eng. 82 (2018) 322-330.
[17] S.N. Basahel, T.T. Ali, M. Mokhtar, K. Narasimharao, Nanoscale Res Lett. 10 (2015)73–86.
[18] N.W.C. Jusoh, A.A. Jalil, S. Triwahyono, C.R. Mamat, Appl. Catal. A: Gen. 492 (2015) 169–176.

[19] N. Rani, R. Ahlawat, B. Goswami, Mater Chem Phys. 241 (2020) 122401
[20] F.F.A. Aziz, A.A. Jalil, S. Triwahyono, M. Mohamed, Appl Surf Sci. 455 (2018) 84–95.
[21] M. Aflaki, & F. Davar, J Mol Liq, 221 (2016) 1071–1079.
[22] C.N.C. Hitam, A.A. Jalil, S. Triwahyono, A.F.A. Rahman, N.S. Hassan, N. F. Khusnun, A. Ahmad, Fuel. 216 (2018) 407–417.
[23] R. Saravanan, S. Agarwal, V.K. Gupta, M.M. Khan, F. Gracia, E. Mosquera, V. Narayanan, A. Stephen, J. Photochem. Photobiol., A 353 (2018) 499–506.
[24] N.F. Jaafar, A.A. Jalil, S. Triwahyono, Appl. Surf. Sci. 392 (2017) 1068-1077.
[25] C.N.C. Hitam, A.A. Jalil, S. Triwahyono, A. Ahmad, N.F. Jaafar, N. Salamun, Z. Ghazali, RSC Adv. 6 (2016) 76259–76268.

Malaysian Journal of Catalysis
http://mjcat.utm.my/
MJCat
Research Article

Synthesis and Characterization of Titanium Catalyst Containing Polystyrene Composites for Epoxidation Of 1-Octene

Mohd Hayrie Mohd Hatta[1*], Juan Matmin[2], Hadi Nur[2,3], Kalaivani Batumalaie[4]

[1]*Centre for Research and Development, Asia Metropolitan University, 81750 Johor Bahru, Johor, Malaysia*
[2]*Department of Chemistry, Faculty of Science, Universiti Teknologi Malaysia, 81310 UTM Johor Bahru, Johor, Malaysia*
[3]*Centre for Sustainable Nanomaterials, Ibnu Sina Institute for Scientific and Industrial Research, Universiti Teknologi Malaysia, 81310 UTM Johor Bahru, Johor, Malaysia*
[4]*Department of Biomedical Sciences, Faculty of Health Sciences, Asia Metropolitan University, 81750 Johor Bahru, Johor, Malaysia*

**Corresponding Author: hayrie@amu.edu.my*

Article history :
Received 21 September 2021
Accepted 4 October 2021

GRAPHICAL ABSTRACT

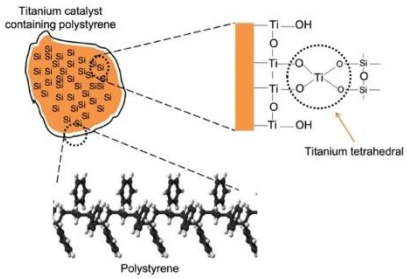

ABSTRACT

The titanium catalyst containing polystyrene composites have been prepared by reacting titanium (iv) isopropoxide (TTIP) with octadecyllthrichlorosilane (OTS) under ambient atmosphere with absence and presence of water. The resulting catalysts were characterized by diffuse reflectance ultraviolet-visible (DR UV-Vis) spectroscopy, X-ray diffraction (XRD) spectroscopy, field emission scanning electron microscopy (FESEM) attached with energy dispersive X-ray (EDX) spectroscopy, Fourier transform infrared spectroscopy (FTIR) and ^{29}Si Magic Angle Spinning Nuclear Magnetic Resonances (^{29}Si MAS NMR). XRD patterns demonstrated that the as-synthesized titanium containing catalysts were in amorphous phase. DR UV-Vis analysis showed that the shifting of absorption spectra to shorter wavelength indicated that more titanium tetrahedral species were formed when the amount of water was increased. This result suggests that the presence of water during the reaction between TTIP and OTS has facilitated the formation of Ti – O – Si bond. The formation of Ti – O – Si bonds were also supported by NMR studies which demonstrated a peak shifting from lower to higher intensity in -40 ppm, which corresponds to the formation of Q^2. The as-prepared catalyst with the high content of titanium tetrahedral (0.5-TS) was selected as catalyst in polymerization of styrene in the presence of aqueous hydrogen peroxide (H_2O_2). The polymerization of styrene using the 0.5-TS produced the polystyrene-TiO_2 composite. The catalytic performance of polystyrene TiO_2 composites have been evaluated in the epoxidation of 1-octene in the presence of aqueous H_2O_2. However, it was demonstrated that the catalytic activity of polystyrene TiO_2 composites did not improve much as 17.3 mmol of 1,2-Epoxyoctane was obtained, a slight increase of 0.5% when compared to that of unmodified TiO_2.

Keywords: Epoxidation; Titanium containing polystyrene catalyst; Titanium(iv) isopropoxide; Octadecylthrichlorosilane; Octene Polymerization of styrene.

| eISSN 0128-2581 |

1. INTRODUCTION

Catalyst is as a substance that can be added to a particular reaction to increase the rate of reaction without getting consumed in the process [1]. Generally, the catalysis can be divided into two categories; a homogeneous catalyst where the catalyst is in the same phase as the reaction mixture and heterogeneous catalysis where the catalyst and the reactants are in different phases. [1,2]. Homogenous catalyst is used over heterogeneous catalyst owing to it has more catalytical sites which give improved selectivity to a certain product. However, the difficulty in filtering the catalysts from the reaction media has limited the application of homogeneous catalysts in the industry. In addition, separation approaches such as distillation require an extra expenditure of energy and high-cost production [3, 4].

Like a homogenous catalyst, the heterogeneous catalyst also has its own drawbacks. For example, availability of surface area for reaction sites, limited activity and selectivity, and high cost in the production of catalyst. Therefore, a newly designed catalyst is expected to be commercially and economically viable. These include fabrication of low-cost catalysts, fulfil the objectives for ease of construction and dependability of operation [3-5]. The principle of this research is to design and fabricate a new catalyst that will increase the surface-active site and the interests of the research remains in the field of preparation, characterization and evaluation of the catalytic performance.

For over the last decades, titanium silicate (TS-1) has been widely used as a catalyst in epoxidation with hydrogen peroxide owing to its high activity and selectivity [6]. The synthesis of organic compounds to produce industrial materials based on epoxidation reaction which used TS-1 as a catalyst has shown an excellent result. Epoxides can be considered as useful intermediates that are widely applied in organic synthesis. Thus, the epoxidation of hydrocarbon compounds such as alkenes is important in research and development as well as in industrial applications [6,7]. Despite the excellent properties of TS-1 as a catalyst in the chemical industry, the large pore size has limited their application in the fabrication of large organic compounds. Therefore, TS-1 is only highly selective for catalysis of the small molecules [7-9].

Previous research that has been carried out showed that titania-silica mixture has successfully polymerized the styrene to form titanium catalyst containing polymer composites [10]. The titania composite was demonstrated to comprise high content of tetrahedral titanium which improve its catalytic activity. In addition, the presence of polymer in the catalyst can be utilised as fillers to enhance the strength, processability, and thermal stability [11, 12]. The concept is based on the idea that titanium catalysts containing polymer composites formed in the solid phase will be utilised as catalyst in the epoxidation of alkene. With these properties, polystyrene would be able to activate the active site by creating the active site with more electrophilic properties. Thus, it would be easier for the composites to be attacked by nucleophile such as alkenes [13]. Therefore, this study proposed to synthesize the titanium catalyst containing polystyrene with using titanium (IV) isopropoxide and octadecylthriclorosilane (OTS) as source of titania and silica. The prepared TiO_2-SiO_2 catalysts would then introduce with polystyrene to produce the titanium catalyst containing polystyrene for the application in epoxidation of 1-octene with the presence of hydrogen peroxide.

2. EXPERIMENTS

2.1 Preparation of titania-silica catalyst

The titania-silica catalysts were prepared by addition of 1.267 ml of titanium(iv) isopropoxide, TTIP (97%, Sigma-Aldrich) and 3.967 ml of octadecyltrichlorosilane, (>90%, Sigma-Aldrich) under ambient atmosphere with absence and presence of water (H_2O). The amount of water added into the reaction was varied to 0.25 ml, 0.50 ml, 1.00 ml, 2.5 ml and 5.0 ml. The toluene (95%, Merck) was used as a solvent in the synthesis step. The experiment was performed in a fume hood to avoid evaporation of compounds and was placed in an ultrasonic bath for 2 hours to complete the hydrolysis process. The mixture was then washed with methanol, CH_3OH, (99.8%, HmBG Chemical) up to three times to remove chloride ions. The prepared titania-silica samples were denoted as following; TS, 0.25-TS, 0.5-TS, 1.0-TS, 2.5-TS and 5.0-TS, respectively.

2.2 Preparation of titanium catalyst containing polystyrene composite

For the preparation of titanium catalysts containing polystyrene composite. A 100 mg of TS catalyst was added to 10.42 g of styrene in a 100 ml round bottom flask. An amount of 0.68 ml (10 mmol) of hydrogen peroxide, H_2O_2, (99%, Sigma-Aldrich) was added to the reaction. The mixture was then stirred at the temperature of 80 °C for eight (8) hours to undergo a reflux process. The mouth of condenser was covered with aluminium foil to prevent the mixture from evaporating. The experimental was repeated using 0.25-TS, 0.5-TS, 1.0-TS, 2.5-TS and 5.0-TS catalysts, respectively. The final composites (titanium catalyst containing polystyrene) were denoted as TS-PS, 0.25-TS-PS, 0.5-TS-PS, 1.0-TS-PS, 2.5-TS-PS and 5.0-TS-PS, respectively.

2.3 Characterization

The structural studies of prepared titania-silicate catalysts were characterized by X-ray diffraction (XRD) spectrometer using Bruker D8 Advance with CuK_a irradiation and wavelength of 1.5406Å. Optical studies were performed using Perkin Elmer Lambda 900 diffuse reflectance ultraviolet-visible (DR UV-Vis) spectrophotometer with wavelength recorded from 200 – 800 nm to study the phase of titania. In addition, the ^{29}Si magic angle spinning nuclear magnetic resonance, (^{29}Si MAS NMR) was used to study the Ti-O-Si linkages using Bruker Avance 400 MHz solid-state NMR. Investigation on the formation of Ti and Si bonds were also carried out using the Perkin Elmer Fourier transform infrared (FTIR) spectrometer. The KBr pellets technique was used in this analysis. The morphological properties of prepared catalysts were studied by field emission scanning electron microscope, FESEM (JSM-6330F).

2.4 Catalytic Activity

In this study, the catalytic performance of TiO_2, 5.0-TS and 5.0-TS-PS were evaluated in the epoxidation of 1-octene (99%, Sigma-Aldrich). The catalytic testing was carried out by mixing the 100 mg of the catalyst with 4 ml of 1-octene and 1 ml of hydrogen peroxide. The catalytic reactions were conducted at the temperature of 80 °C for eight (8) hours. The final product was analysed using gas chromatography with a flame ionization detector, GC (Agilent Ultra-1). For comparison, the epoxidation of 1-octene was also carried out without the presence of any catalysts.

3. RESULTS AND DISCUSSION

Fig. 1 shows the XRD patterns of the prepared titania-silica catalysts. Two major peaks were observed which were in low angle (2 - 10°) and high angle (21 - 24°).

At a lower angle, the appearance of three peaks with low intensity were corresponded to be (100), (111) and (220) planes. The appearance of the respective planes was corresponded to the formation of mesostructured materials or 2D-hexagonal mesophase [14]. The decreased intensity of the peaks associated with the planes as the amount of water increased might be due to the formation of individual titania and silica small particles that embedded in the mesostructured frameworks. Thus, affecting the mesostructured frameworks. The formation of titania and silica particles were due to the self-hydrolysis and condensation of individual TTIP and OTS [15, 17]. Meanwhile, the broad peak at *ca.* 2*q* of 22.1° was attributed to the presence of silica in the amorphous phase [15-17]. The absence of TiO_2 diffractograms possibly due to the low amount of titania presence in the samples. It was reported that titania-silica materials consist of two phases which are amorphous and mesostructured [16, 17]. Since all the diffractograms showed a similar pattern, it can be concluded that the addition of water did not affect the degree of crystallization of TS.

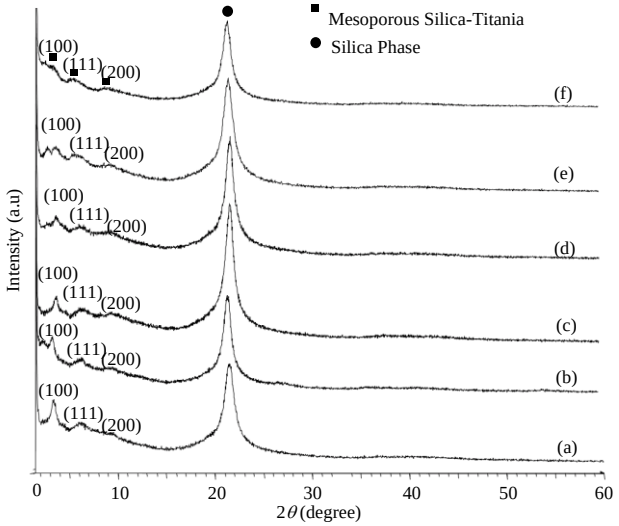

Fig. 1. XRD patterns of (a) TS, (b) 0.25-TS, (c) 0.5-TS, (d) 1.0-TS, (e) 2.5-TS and (f) 5.0-TS

The optical studies of the prepared catalysts were investigated using DR UV-Vis spectroscopy. The peak in the range of *ca.* 200 – 260 nm was attributed to a charge transfer of titanium tetrahedral while octahedral species showed an appearance peak at *ca*. 280 – 330 nm [17]. As shown in the Fig. 2, increasing the amount of water (Fig. 2(b)-(f)) caused the absorption spectra to shift to the shorter wavelength. The preparation of titania-silica catalysts with lesser amount of water (Fig. 2(b)-(c)), resulted in lower formation of titanium tetrahedral. Hence, the peak at *ca.* 280 – 330 nm, which corresponded to the titanium octahedral species was more prominent. These results suggest that the presence of water play a key role in the formation of titanium tetrahedral. However, the preparation of titania-silica catalyst without any addition of water (Fig. 2(a)) showed a prominent absorption peak at *ca.* 200 – 260 nm, which corresponded to the formation of titanium tetrahedral species. Without any addition of water, the titanium octahedral species are supposed to dominate the sample instead of tetrahedral species. Although the reason is still unclear, the formation of tetrahedral species might be due to a long hydrolysis process of TTIP and OTS that it was possible for the reaction to absorb moisture from the environment. Thus, leading to the formation of titanium tetrahedral species. In addition, it has been reported in the literature [17] that preparation of titania-silica catalyst without addition of water produces a TiO_2 cluster containing OH groups that makes the catalyst more hydrophilic.

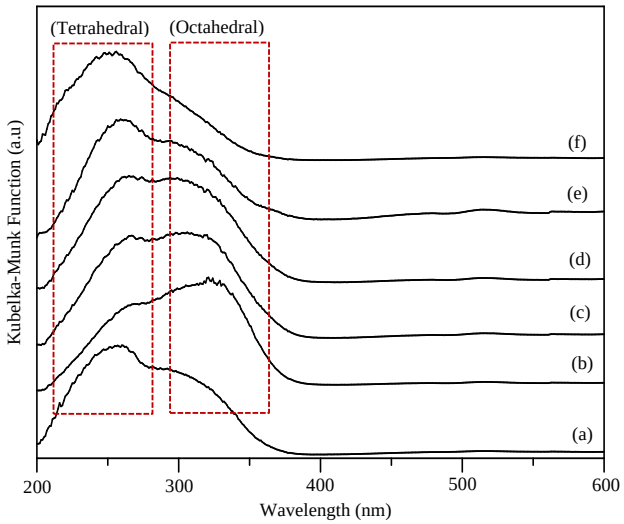

Fig. 2. DR UV-Vis spectra of (a) TS, (b) 0.25-TS, (c) 0.5-TS, (d) 1.0-TS, (e) 2.5-TS and (f) 5.0-TS

The morphological properties of the prepared TS and 5.0-TS catalysts were shown in Fig. 3 and Fig. 4. The FESEM images of both samples show that the catalysts were in irregular shape with the agglomeration of individual particles on the surface of catalyst. With addition of water (Fig. 4(b)), less agglomeration of particles was observed on the surface, suggesting the formation of more Ti – O – Si bonds in the catalyst. The Ti and Si mapping by EDX show that both samples were composed of TiO_2 cluster and SiO_2 small particles. The formation of TiO_2 clusters and SiO_2 particles were resulted from self-hydrolysis and condensation of individual TTIP and OTS [17]. Thus, these findings were in agreement with the decreased intensity of XRD peaks related to the mesostructured frameworks (**Fig. 1**). In addition, it can be observed that the SiO_2 particles were distributed homogeneously on the surface of both samples. As shown in Fig. 4(b), the intensity of TiO_2 cluster in sample 5.0-TS was slightly reduced when compared to that of

sample TS. These results suggest that the addition of water facilitate the formation of Ti and Si bonds. The EDX analysis as shown in Fig. 5 demonstrated that the composition of Si was much higher that Ti, thus supporting the reason why the titania peaks were not detected in XRD diffractograms. It was also observed that the composition of chloride ions (Cl^-) in both catalysts were below 1%, suggesting the methanol can be an effective treatment in removing Cl^- ions.

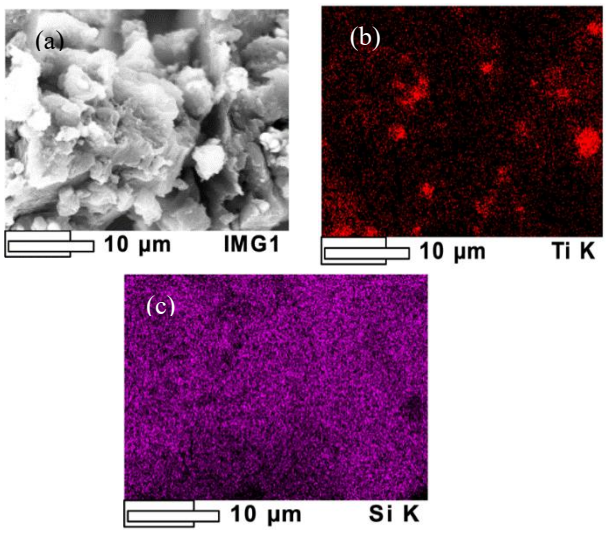

Fig. 3. The (a) FESEM micrograph and EDX mapping of (b)Ti and (c) Si for sample TS

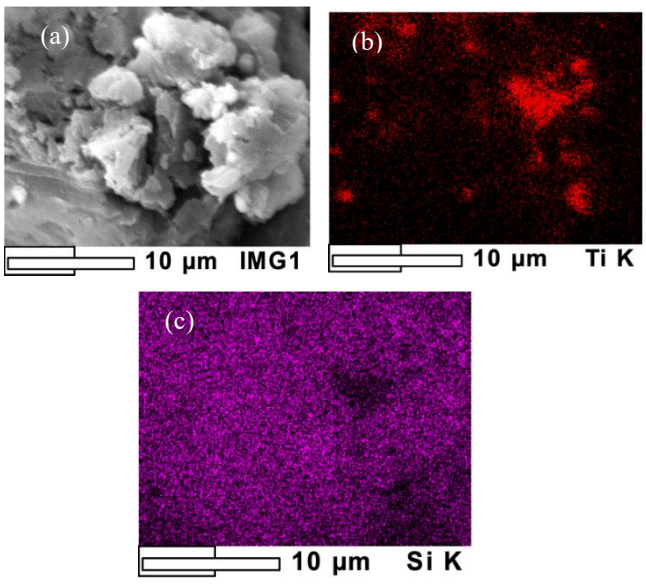

Fig. 4. The (a) FESEM micrograph and EDX mapping of (b)Ti and (c) Si for sample 5.0-TS.

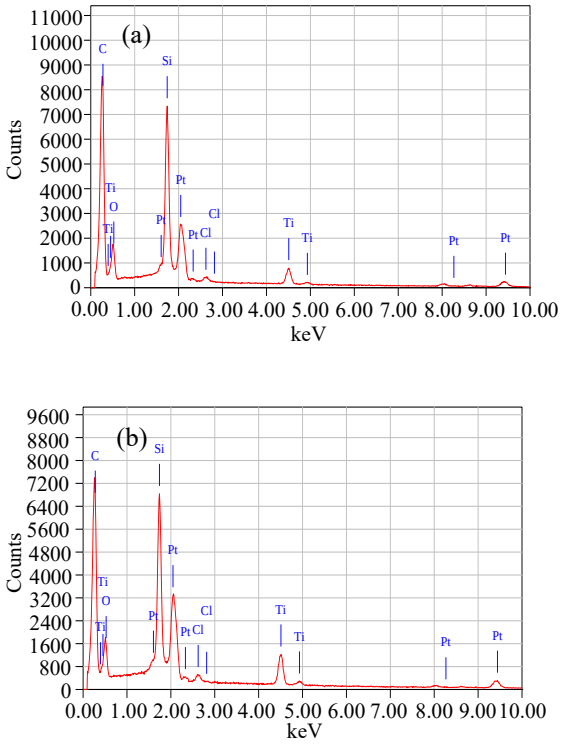

Fig. 5. Elemental analysis of: (a) TS and (b) 5.0-TS.

Fig. 6 shows the spectra of ^{29}Si Magic Angle Spinning Solid Nuclear Magnetic Resonance (MAS Solid NMR). As shown in the figure, *T* denominates the presence of corresponding Si sites in spectra. T^3 peak was corresponded to the formation of $C_{18}H_{37}Si(OSi)_3$ while T^2 indicated to formation of $C_{18}H_{37}Si(OTi)(OSi)_2$ [18]. It was demonstrated that increasing the amount of water led to an increase in the intensity of T^2, suggesting the increase in the formation of titanium tetrahedral in the catalyst.

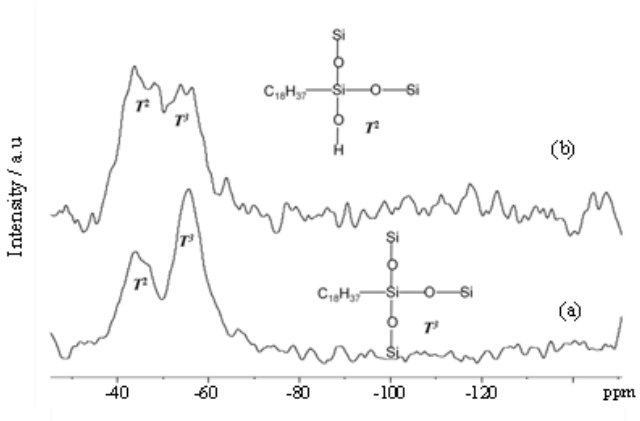

Fig.6. ^{29}Si MAS NMR spectra for (a) 0.25-TS and (b) 5.0-TS.

FTIR studies were carried out in order to determine the chemical bonds and functional groups of the prepared TS catalysts. Based on Fig. 7, the broad peak in the region of 3000 – 4000 cm^{-1} was corresponded to the bending and stretching mode of O-H of silanol group, respectively [19]. It was observed that increasing the amount of water led to a decrease in the peak intensity of OH. The decrease in the peak intensity was due to the conversion of O-H group to Ti – O – Si bond. The successful formation of Ti – O – Si can be observed from the peak that appeared at region of *ca*. 950 cm^{-1} [20]. The presence of Ti – O – Si bond in TS catalyst was possible due to the absorption of water from the environment during the hydrolyzation process. Thus, explain the formation of Ti – O – Si in the catalyst.

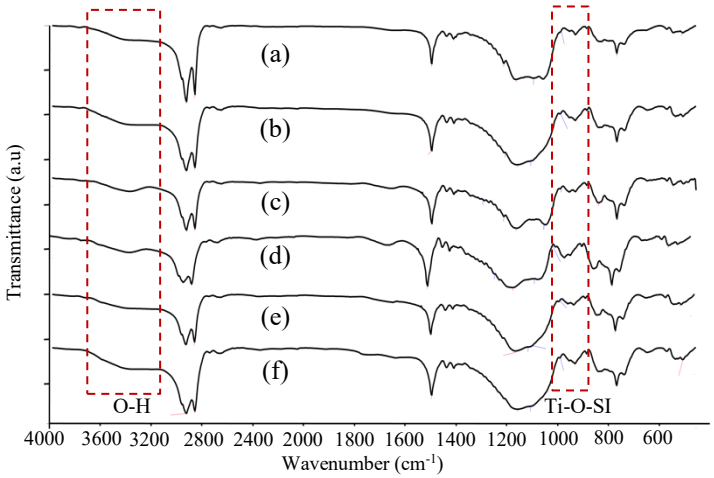

The catalytic activity of the prepared catalysts was evaluated in the epoxidation of 1-Octene. For comparison, the epoxidation of 1-Octene with the presence of hydrogen peroxide without addition of catalyst was also conducted (Fig.8(a)). The product of 1-Octene epoxidation which was 1,2-Epoxyoctane was also analysed as a reference by gas chromatography. Based on the GC analysis, the retention times of the sample appeared after the sixth minute. The observed peak was corresponded to 1,2-Epoxyoctane as according to the retention time of reference. As shown in Fig. 8(a), there was no amount of 1,2-Epoxyoctane detected, suggesting the epoxidation of 1-Octene could not be performed without a catalyst. When TiO_2 was used as catalyst, about 17.2 mmol of 1,2-Epoxyoctane was obtained. However, the catalytic activity was dropped to 12.4 mmol when titania-silica (5-TS) was used a catalyst. A slight increase in catalytic activity was demonstrated by sample 5-PS-TS composite as 17.3 mmol of 1,2-Epoxyoctane was obtained. These findings suggest that the titanium containing polystyrene composite has slightly improved the catalytic performance of TiO_2. Although the reason for the decrease in the catalytic activity of 5-TS is not entirely clear, it is suggested that the small particles of SiO_2 which were distributed homogeneously on the surface of the sample have reduced the catalytic active sites for the material. The formation of small particles of SiO_2 as demonstrated by EDX mapping (Fig. 3 and 4) were resulted from the self-hydrolysis and condensation of individual OTS and TTIP during hydrolysis process. It can be suggested that the introduction of polystyrene in the titania-silica has slightly improved back the composite performance in catalytic testing. Therefore, more findings and analyses are required in order to fully conclude the effectiveness of polymer in improving the catalytic properties of TiO_2.

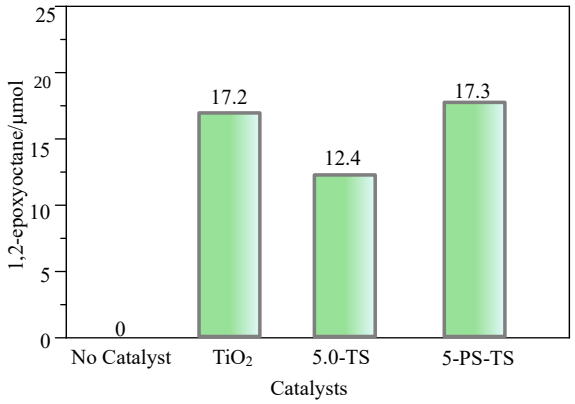

Fig. 8. Catalytic activity of (a) without catalyst (b) TiO_2, (c) 5.0-TS and (d) PS-TS

4. CONCLUSION

Titanium catalyst containing polystyrene composites have been successfully prepared by polymerization of styrene using titania-silica catalyst. The catalysts were prepared first by mixing the titanium(iv) isopropoxide (TTIP) and octadecyltrichlorosilane (OTS) in toluene as solvent. The role of water in formation of Ti and Si bond was investigated by the different amounts of water added to the mixture of TTIP and OTS. The DR UV-Vis and NMR studies showed that the formation of Ti – O – Si bonds were facilitated by the addition of water. Hence, more tetrahedral titanium active sites were produced. The presence of titanium tetrahedral in the titania-silica catalyst and electrophilic properties of polystyrene were expected to improve the catalytic performance of the composite in epoxidation of 1-Octene. The catalytic testing demonstrated the prepared composite slightly improved the catalytic activity of unmodified TiO_2. However, the formation of individual SiO_2 particles on the surface of catalyst during self-hydrolysis of OTS and TTIP may result to the decrease in its catalytic activity as it would reduce the catalytic active sites. For future studies, it is recommended to improve the technique in the preparation of titania-silica catalysts to obtain catalyst with high content of titanium tetrahedral species.

ACKNOWLEDGEMENTS

We gratefully acknowledge the research funding from Universiti Teknologi Malaysia (UTM) via UTMER (Cost Centre Code: UTMER Q.J130000.2654.18J18).

REFERENCES

[1] P. Atkins, JD Paula, Atkins' Physical Chemistry. Oxford University Press, 2006 p, 839.
[2] P. Dyson, DJ. Ellis, T. Welton, Biphasic Homogenous Catalyst, Platinum Metal Rev, 42:4 (1998), 135-140.
[3] JT Richardson, Principles of Catalyst Development, Plenum Press, New York, 1989, 1-8.
[4] H. Nur, Heterogenous Chemocatalysis: Catalysis by Chemical Design. Ibnu Sina Institute for Fundamental Science Studies. Penerbit Universiti Teknologi Malaysia. 2006, p, 5-10.
[5] H. Nur, S. Ikeda, B. Ohtani, Akademiai Kiado, Budapest. 82:2 (2006), 255- 261.
[6] DM. Chapman, AL. Roe, Zeolites, 10(1990), 730-731.
[7] AJ. Bonon, D. Mandelli, OA. Kholdeeva, MV. Barmatova, YN. Kozloz, GB. Shulpin, Applied Catalysis A: General, 365(2009), 96–104.
[8] C. Cativiela, JM. Fraile, JI. Garcia, JA. Mayoral, Journal of Molecular Catalysis A: Chemica, 112(1996), 259-267.
[9] Z. Qian, L. Ping, L. Daoquan, Z. Xinggui, Y. Weikang, H. XiJun, Microporous and Mesoporous Materials, 108(2007), 311-317
[10]K. Kang, H. Rhee, Studies in Surface Science and Catalysis, 159(2006), 789-792.
[11] TP. Selvin, JS. Kuruvilla, Materials Letters, 58(2004), 281– 289
[12] S. Samsudin, A. Hassan, M. Mokhtar, S. Syed Jamaluddin, (2006). 1:1(2006), 11-24.
[13] TP. Selvin, JS. Kuruvilla, Materials Letters, 58(2004), 281– 289
[14] OK, Kholdeeva, NN. Trukhan, Russ. Chem. Rev. 75(5), (2006) 411–432.
[15]Y. Mori, Y. Okastu, Y. Tsujimoto, Journal of Nanoparticle Research, 3(2), (2001) 219-225.
[16] D. Comedi, O.H.Y. Zalloum, E. Irving, J. Wojcik, T. Roschuk, M.J. Flynn, P. Mascher, J. Appl. Phys. 99 (2) (2006) 023518-1–023518-8.
[17]UK. Nizar, J. Efendi, L. Yuliati, D. Gustiono, Nur, H, Chem Eng J, 222(2013), 23-31.
[18] H. Nur, Materials Science and Engineering B, 133(2006). 49-54.
[19] S. Cao, K.L. Yeung, P-L. Yue, Appl. Catal. B 68 (2006) 99–108.
[20]Ikeue, K., Ikeda, S., Watanabe, A., Ohtani, B. (2004). Phys.Chem.Chem.Phys., 6, 2523–2528.

Malaysian Journal of Catalysis
http://mjcat.utm.my/
MJCat Research Article

$CuFe_2O_4$ as a heterogeneous Fenton catalyst for the removal of ciprofloxacin from aqueous solution at natural pH

Nurul Najwa Mohamad Jani[a], Saifullahi Shehu Imam[b*], Alamri Rahmah Dhahawi Ahmad[a], Rohana Adnan[a*]

[a]*School of Chemical Sciences, Universiti Sains Malaysia, 11800, Penang, Malaysia*
[b]*Department of Pure and Industrial Chemistry, Bayero University P.M.B 3011, Kano, Nigeria*

**Corresponding Author: r_adnan@usm.my; ssimam.chm@buk.edu.ng*

Article history :
Received 29 September 2021
Accepted 14 November 2021

GRAPHICAL ABSTRACT

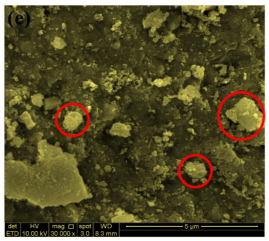

ABSTRACT

In the present study, a bimetallic oxide catalyst of $CuFe_2O_4$ was synthesized via facile co-precipitation process and characterized using various techniques such as X-ray diffraction (XRD), Fourier transform infrared spectroscopy (FTIR), field emission scanning electron microscope (FESEM), energy dispersive X-ray (EDX), N_2 adsorption – desorption analysis and UV-visible spectroscopy. Subsequently, it was used to degrade ciprofloxacin (CIP), a fluoroquinolone antibiotic, from an aqueous solution via the Fenton process under various conditions. The effect of several operational parameters such as catalyst dosage, H_2O_2 volume, initial CIP concentration, inorganic ions, and solar irradiation has also been evaluated. The removal process was found to follow the trend: photo-Fenton > Fenton > catalytic > adsorption > photolysis. The results showed that the $CuFe_2O_4$ catalyst degraded a high percentage of CIP and maintained reasonable efficiency even after five cycles, thus indicating that $CuFe_2O_4$ is a promising catalyst for the activation of H_2O_2 to degrade antibiotics.

Keywords: $CuFe_2O_4$; Heterogeneous catalyst; Fenton oxidation; Ciprofloxacin; Wastewater treatment.

| eISSN 0128-2581 |

1. INTRODUCTION

Ciprofloxacin (CIP) is a second-generation quinolone antibiotic widely used for medical treatments due to its strong antibacterial activity [1]. However, CIP is only partially metabolized by the body after ingestion, and around 20% - 80% of the drug is excreted back in pharmacologically active form into the water bodies [2-4]. Its presence in water has been reported to inhibit the growth of spinach plants, affect non-intended pathogens, lead to the development of antibiotic-resistant bacteria, and the risk of consuming water contaminated by CIP [5-7]. Unfortunately, studies have shown that traditional wastewater treatment techniques do not remove low CIP concentrations [8]. Thus, it is critically essential to exploit more effective methods for the removal of CIP.

Fenton process is one of the most famous advanced oxidation processes (AOPs), which has attracted significant attention due to its low toxicity, high efficiency, and simple operation [9]. The process initially involves the generation of reactive oxygen species (specifically hydroxyl radicals ($^{\bullet}OH$)) via catalytic decomposition of H_2O_2 by Fe^{2+} (Eq. 1). Subsequently, regeneration of Fe^{2+} is possible via the reduction of Fe^{3+} using H_2O_2 (Eq. 2) [10]. Nowadays, researchers have focused more on heterogeneous Fenton catalysis due to the ease of recovery of the catalyst [11].

$$Fe^{2+} + H_2O_2 \rightarrow Fe^{3+} + {}^{\bullet}OH + {}^{-}OH \quad k_1 = 40 - 80\ M^{-1}s^{-1} \qquad (1)$$

$$Fe^{3+} + H_2O_2 \rightarrow Fe^{2+} + HO_2^{\bullet} + H^{+} \quad k_2 = 0.001 - 0.01\ M^{-1}s^{-1} \qquad (2)$$

$CuFe_2O_4$ is a spinel ferrite with high catalytic performance and is catalytically more stable than $CuFeO_2$ [12, 13]. It is commonly used as a catalyst in hydrogen production from oxygenated hydrocarbons [14], decomposition of gaseous pollutants [15], water gas shift reaction [16], and in activating oxidizing agents [17]. In the current study, $CuFe_2O_4$ would be prepared via a facile co-precipitation process and characterized using various techniques. Subsequently, the catalytic ability and stability of $CuFe_2O_4$ would also be evaluated by removing CIP antibiotics from an aqueous solution.

2.0 MATERIALS AND METHODS

2.1 Chemicals

All chemicals were analytical grade and were used without further purification. Copper (II) nitrate trihydrate ($Cu(NO_3)_2{\cdot}3H_2O$), iron (III) nitrate nonahydrate ($Fe(NO_3)_3{\cdot}9H_2O$), sodium hydroxide (NaOH), hydrogen peroxide (H_2O_2, 30%), sodium nitrate ($NaNO_3$) and sodium bicarbonate ($NaHCO_3$) were supplied by QReC (Asia). Sodium sulphate anhydrous (Na_2SO_4) and sodium chloride (NaCI) were from Bendosen Laboratory Chemicals. Ciprofloxacin ($C_{17}H_{18}FN_3O_3$) was obtained from Fluka Chemicals. Distilled water was used during the preparation of all solutions.

2.2 Synthesis of $CuFe_2O_4$

$CuFe_2O_4$ was prepared using the method reported by Hegazy *et al.* [18] with slight modifications. As much as 0.025 moles of copper nitrate ($Cu(NO_3)_2{\cdot}3H_2O$) and 0.05 mole of iron nitrate ($Fe(NO_3)_3{\cdot}9H_2O$) were dissolved together in a beaker containing 100 mL of distilled water under continuous stirring at room temperature. The precipitation reaction was performed by adding 75 mL of 4 M sodium hydroxide solution dropwise into the above mixture with moderate stirring and reaction temperature maintained at 90 °C for 3 hours. The resulting product was filtered and washed several times with distilled water until a constant pH of ~8 was attained. The product was then dried at 60 °C in an oven overnight. Subsequently, the dried product was grounded, and calcination was performed at 400 °C for 4 hours with a heating rate of 10 °C/min under an air atmosphere. The resulting product was blackish $CuFe_2O_4$ powder.

2.3 Characterization

The crystal structure of $CuFe_2O_4$ was characterized using X-ray powder diffractometer (BRUKER D8) with Cu-Kα radiation over 2θ scanning range of 10 – 90º. Surface morphology and elemental composition were investigated using Carl Zeiss Leo Supra field emission scanning electron microscope (FESEM) with Oxford instrument X-max Energy dispersive X-ray (EDX). UV-vis analysis was conducted using Perkin Elmer Lambda 35 spectrometer equipped with diffuse reflectance attachment. FTIR spectra was measured using Perkin Elmer 2000 in the wavenumber range of 400 – 3600 cm^{-1}. The specific surface area of $CuFe_2O_4$ was determined using Micromeritics ASAP 2020 V 4.01 at liquid nitrogen temperature (-196 ºC).

2.4 Removal study

All experiments were conducted using a constant working liquid volume of 100 mL in 250 mL glass beakers. The effect of catalyst dosage was conducted by using various amounts of $CuFe_2O_4$ (0.25, 0.50, 0.75, 1.0, 1.25 and 1.50 g/L) and 0.5 mL 30% H_2O_2 for degrading 20 mg/L of CIP. To investigate the effect of volume of H_2O_2, experiments were carried out by adding either 0.3, 0.5, or 0.7 mL of 30% H_2O_2 to 20 mg/L CIP solution with 1.0 g/L catalyst dosage. The effect of initial CIP concentration was studied by adding 1.0 g/L of $CuFe_2O_4$ and 0.5 mL of 30% H_2O_2 to 100 mL of 5, 10, 15, 20, 30, and 40 mg/L of CIP solutions. Since organic pollutants and inorganic ions often coexist in real wastewater, the effect of inorganic ions on the degradation of 20 mg/L aqueous CIP solution using 0.5 mL of 30% H_2O_2 was carried out by adding 10 mM of either NaCl, $NaNO_3$, $NaHCO_3$, or Na_2SO_4 salts. The effect of solar irradiation on the Fenton/catalytic degradation of 20 mg/L aqueous CIP solution was also studied by carrying out reactions under optimized conditions at Penang, Malaysia between 12:00 – 2:00 pm in February 2020. Finally, the used catalyst was recovered for the reusability studies, washed several times with distilled water and ethanol, and dried at 60 ºC overnight in an oven. All experiments were conducted at the natural pH of the aqueous CIP solution, which was 7.10 ± 0.1.

CIP degradation was measured spectroscopically using a Shimadzu UV-2600 UV-Vis spectrometer by withdrawing 5 mL of the reaction suspension, centrifuged immediately at 3500 rpm for 5 min, and the absorbance of remnant CIP was measured at λ_{max} = 276 nm. The percentage of catalytic degradation of CIP was calculated using Eq. 3:

$$\%\ CIP\ removal = \frac{A_o - A}{A_o} \quad (3)$$

where A_o is the initial CIP absorbance before degradation and A is the CIP absorbance after degradation.

3.0 RESULTS AND DISCUSSION

3.1 Characterization of $CuFe_2O_4$ catalyst

Fig. 1(a) shows the XRD pattern of the $CuFe_2O_4$ catalyst. The diffraction peaks at 2θ = 35.5º, 36.9º, 43.2º, 57.8º and 62.2º corresponds to the (311), (222), (400), (511) and (440) planes of cubic $CuFe_2O_4$ (JCPDS NO: 25-0283) respectively [19, 20]. The wide peak at about 2Θ = 23º is an indication that the crystalline structure of $CuFe_2O_4$ combined or interfered over amorphous surroundings [21]. The FTIR spectrum of $CuFe_2O_4$ in the range of 400 – 3600 cm^{-1} is presented in Fig. 1(b). In general, spinel ferrites have two metal-oxygen bands in their spectra. The lower frequency band is usually located within the 450 – 385 cm^{-1} region, while the higher frequency band is found within the 600 – 550 cm^{-1} region [22]. In the case of the $CuFe_2O_4$ catalyst, the peak at about 590 and 440 cm^{-1} are attributed to Fe – O and Cu – O bonds [23]. The band at about 3400 cm^{-1} is due to the hydroxyl functional group, while the peak at 1600 cm^{-1} is due to the bending vibration of adsorbed water molecules [24, 25]. Such results from FTIR have further confirmed the successful $CuFe_2O_4$ synthesis. Fig. 1(c) is the

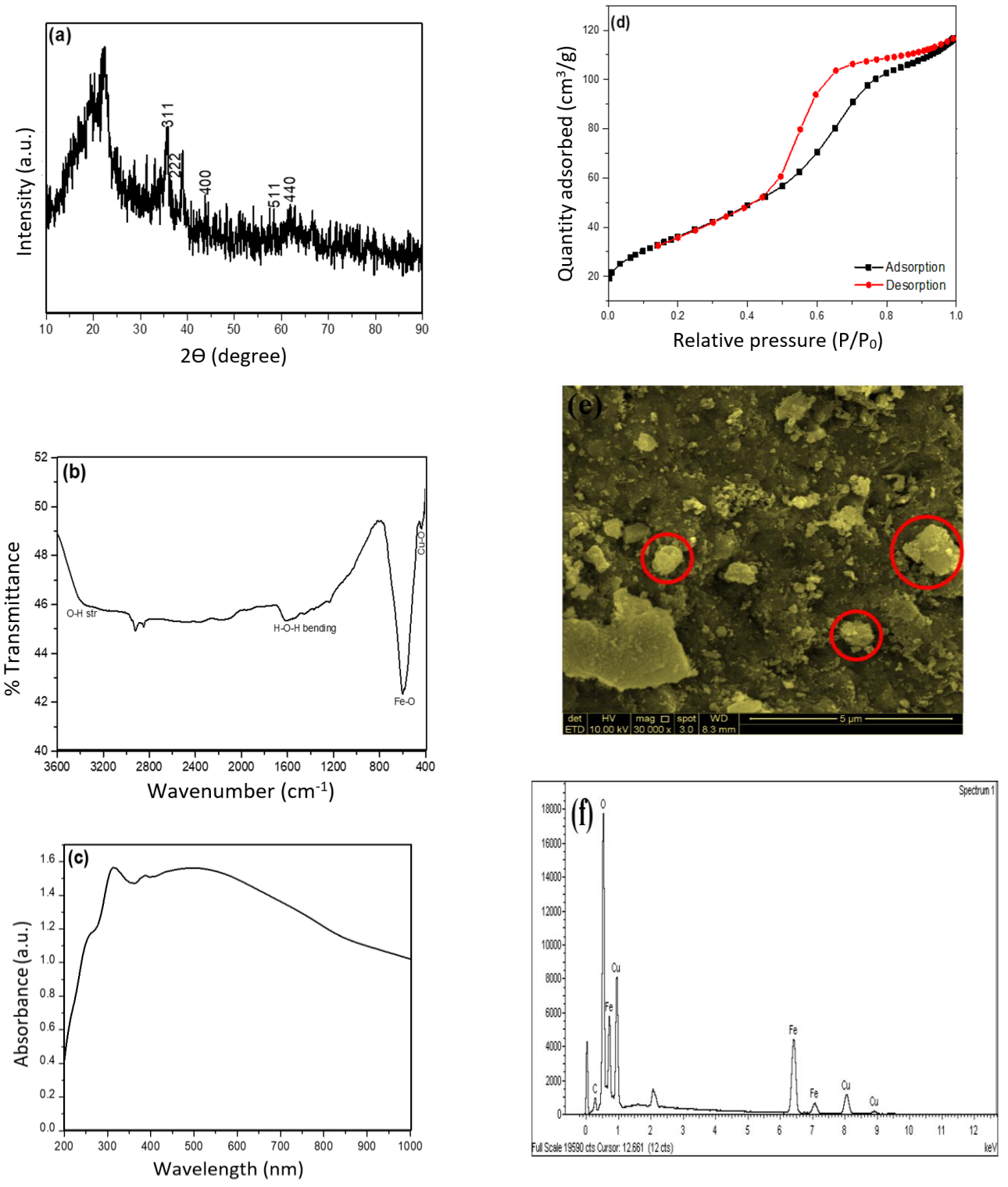

Fig. 1. (a) XRD pattern (b) FTIR spectrum (c) UV-Vis spectrum, (d) N_2 adsorption-desorption isotherm, (e) FESEM image and (f) EDX of $CuFe_2O_4$

absorption spectra of $CuFe_2O_4$, and the absorption band between 310 – 340 nm is assigned to the $CuFe_2O_4$ characteristic bond [26]. In the current study, a band is observed at about 320 nm and is close to the value reported for $CuFe_2O_4$ by Hammad *et al.* [27].

N_2 adsorption-desorption isotherm curve of $CuFe_2O_4$ is shown in Fig. 1(d). Based on the results, the $CuFe_2O_4$ catalyst exhibits a type IV isotherm with H1 hysteresis loop which is attributed to rigid, well-defined, and unconnected pores [28]. The BET surface area of $CuFe_2O_4$ was determined as 120.15 m^2/g. Fig. 1(e) shows the morphology of $CuFe_2O_4$ catalyst consists of irregular and agglomerated particles (some of which have been cycled). The EDX spectra presented in Fig. 1(f) confirm the presence of Cu, Fe, and O in $CuFe_2O_4$. The carbon signal could be due to the adventitious carbon from the atmosphere or the conductive tape used during analysis [29].

3.2 CIP removal process

The effect of various operational parameters such as catalyst dosage, H_2O_2 volume, initial CIP concentration, inorganic ions, and solar irradiation on CIP removal from aqueous solution via heterogeneous catalysis using $CuFe_2O_4$ have been examined and the findings are discussed in the subsequent sections.

3.2.1 Effect of catalyst dosage

The effect of catalyst dosage on CIP removal from aqueous solution via adsorption and heterogeneous Fenton degradation was studied using 0.25 – 1.5 g/L of $CuFe_2O_4$. The results are shown in Fig. 2(a-b). Based on Fig. 2a, the adsorption of CIP using $CuFe_2O_4$ increases with an increase in catalyst dosage. The percentages of CIP removed after 120 min using 0.25, 0.5, 0.75, 1.0, 1.25 and 1.5 g/L of $CuFe_2O_4$ catalyst were 9, 23, 29, 37, 41 and 46%. Such performance is attributed to the increase in active sites and catalyst dosage [30]. Moreover, as the removal percentage remain unchanged after 100 min, it was taken as the equilibrium time for CIP adsorption using different dosages of $CuFe_2O_4$.

In the case of heterogeneous Fenton degradation of CIP in the presence of H_2O_2 using $CuFe_2O_4$ catalyst presented in Fig. 2b, the percentage removal was also found to increase with an increase in catalyst dosage. The percentages removal after 120 min using 0.25, 0.5, 0.75, 1.0, 1.25 and 1.5 g/L of $CuFe_2O_4$ catalyst were 29, 55, 64, 75, 79 and 80%. Such performance could be attributed to the increase in the number of active sites on the catalyst surface, which was projected to accelerate and enhance the hydroxyl radical production by the reactions of hydrogen peroxide decomposition [31]. However, only a slight increase in removal percentage was observed by increasing the catalyst dosage from 1.25 – 1.5 g/L. This could probably be due to the inhibition effect when iron species exist in excess, in which they behaved as scavengers of hydroxyl radicals [32]. Based on the results obtained, the optimum $CuFe_2O_4$ catalyst dosage of 1.0 g/L was used for the rest of the study.

3.2.2 Effect of H_2O_2 volume

The optimization for H_2O_2 was carried out by varying the volumes of H_2O_2 from 0.3 to 0.7 mL, and the results are shown in Fig. 2c. Based on the results obtained, compared to the percentage of CIP removal recorded using 0.3 and 0.7 mL of H_2O_2, the percentage of removal using 0.5 mL of H_2O_2 is higher. From the figure, increasing the H_2O_2 volume from 0.3 to 0.5 mL generally had a positive effect on CIP removal because theoretically, the higher H_2O_2 volume will generate more hydroxyl radical. However, this was not always the case. For instance, the degradation of CIP decreases from 70 to 56% when the volume of H_2O_2 is increased from 0.5 to 0.7 mL. This could be explained by a critical concentration of H_2O_2 in the Fenton process. As the concentration of H_2O_2 increases beyond the critical value, it becomes a hydroxyl radical ($^{\bullet}OH$) scavenger, but the effect is more pronounced at a shorter reaction time, as reported in a previous study [33, 34]. Excess H_2O_2 will also react with $^{\bullet}OH$ to form hydroperoxyl radical ($HO_2^{\bullet}$), with a lower reduction potential value than $^{\bullet}OH$ [35]. The $HO_2^{\bullet}$ can scavenge $^{\bullet}OH$ to form water and oxygen, as shown in Eq. 4 [32]. The recombination of $^{\bullet}OH$ shown in Eq. 5 could also affect the percentage removal if excess H_2O_2 is present [36].

$$H_2O_2 + {}^{\bullet}OH \rightarrow HO_2^{\bullet} + H_2O \quad (3)$$

$$HO_2^{\bullet} + {}^{\bullet}OH \rightarrow H_2O + O_2 \quad (4)$$

$${}^{\bullet}OH + {}^{\bullet}OH \rightarrow H_2O_2 \quad (5)$$

3.2.3 Effect of initial CIP concentration

The study of the dependence of percentage of removal on the initial concentration of the CIP is significant from an application point of view. For this purpose, the dependence of CIP adsorption and degradation on CIP initial concentration has been investigated over the range of 5 to 40 mg/L with an optimum H_2O_2 volume of 0.5 mL. As shown in Fig. 2d, the percentage of removal via adsorption decreases from about 32 to 23% when the concentration of CIP was increased from 10 to 40 mg/L. Such effect is attributed to the high competition for active sites with the increase in initial CIP concentration [37]. In the case of the Fenton degradation process, the percentage of CIP removal using 5 to 30 mg/L does not show much difference and stays around 78-80%. However, when the concentration is 40 mg/L, the removal percentage drops to 70%. The apparent reason for this is that when the initial concentration of the CIP increases, the hydroxyl radical concentrations for all CIP remain constant since the volume of H_2O_2 was fixed at 0.5 mL. Another contributing factor is that at high CIP

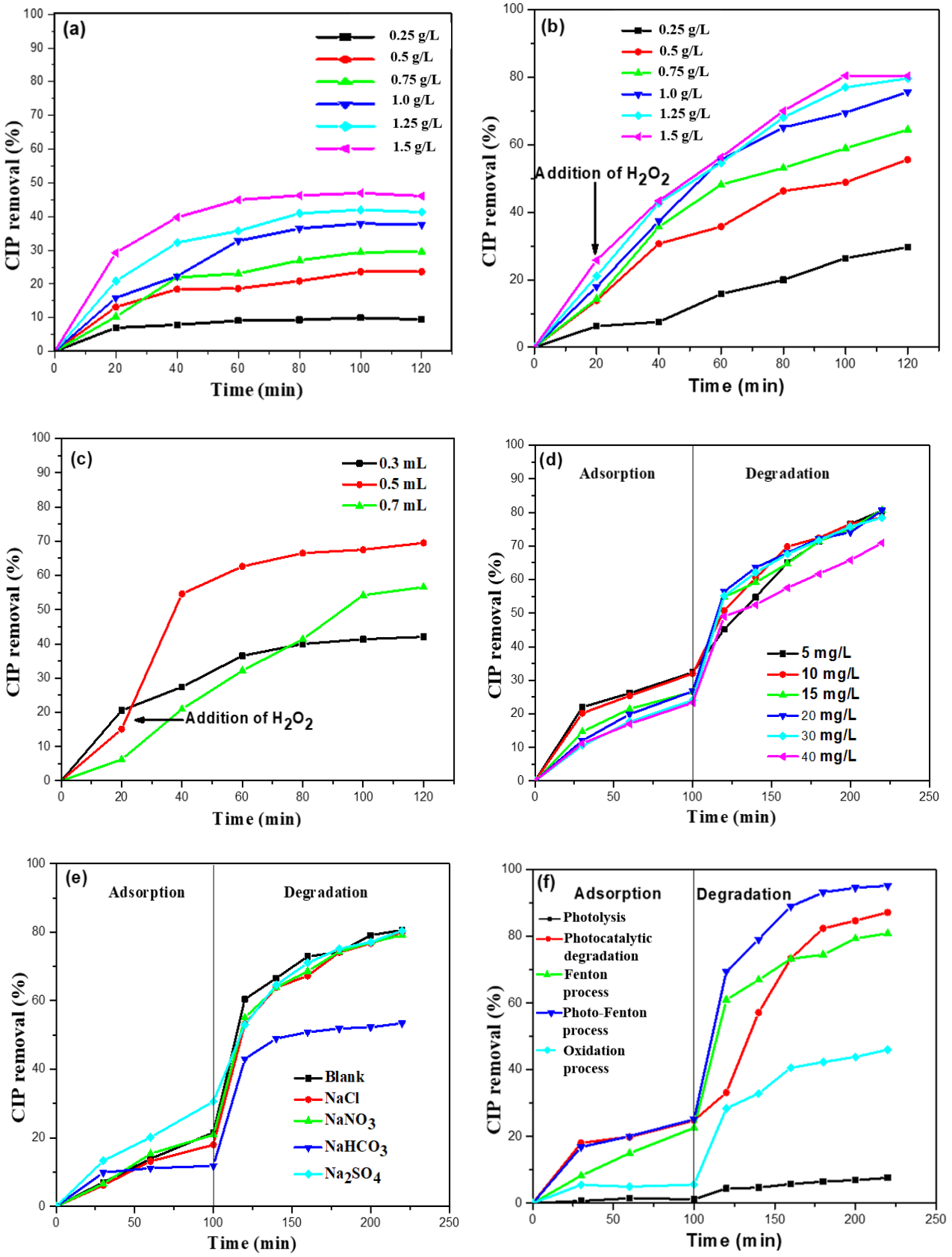

Fig. 2. Effect of some operational parameters on the removal of CIP (a-b) catalyst dosage with and without H_2O_2, (c) volume of H_2O_2, (d) initial CIP concentration, (e) inorganic ions, and (f) solar irradiation.

concentration, the number of active sites available on $CuFe_2O_4$ for hydroxyl radical production by the reactions of hydrogen peroxide decomposition also decreases due to the competitive adsorption of CIP molecules on its surface [38]. The concentration of CIP was set at 20 mg/L to reflect the higher end concentration for antibiotics found in wastewater and treated wastewater [39] and based on the results, it is expected that the catalysts will be efficient to treat CIP at concentrations lower than 20 mg/L.

3.2.4 Effect of inorganic ions

The effect of various inorganic ions such as Cl^-, NO_3^-, HCO_3^- and SO_4^{2-} on the removal of CIP have also been studied, and the results are shown in Fig. 2e. In the presence of Cl^-, NO_3^- and SO_4^{2-}, no significant decrease in degradation efficiency was observed. However, in the presence of HCO_3^-, the percentage removal decreased from 80.6 to 53.4%. This is because HCO_3^- is a hydroxyl radical scavenger which inhibit the degradation of CIP [40].

3.2.5 Effect of solar irradiation

The degradation of CIP in aqueous solution by various processes i.e. photolysis (A), photocatalytic degradation (B), Fenton process (C), photo-Fenton process (D) and oxidation process (E) have been studied, and the results are shown in Fig. 2f. The removal of CIP from aqueous solution via photocatalytic degradation, photo-Fenton, and oxidation processes involves exposure to solar irradiation. The results showed that upon exposure of aqueous CIP solution to solar irradiation but in the absence of $CuFe_2O_4$ or H_2O_2, a very small reduction in CIP concentration (7%) was observed. However, in the presence of $CuFe_2O_4$ i.e. process B, as much as 87% removal was achieved. This showed that $CuFe_2O_4$ has excellent photocatalytic ability to eliminate CIP under solar irradiation. Meanwhile, the degradation of CIP via the photo-Fenton process (D) is more effective than the Fenton process. Up to 95% removal was achieved via the former process compared to only 80% degradation efficiency recorded using the Fenton process (C). It could be possible that the formation of hydroxyl radicals is higher under light exposure (photo-Fenton process) thus leading to a relatively higher degradation efficiency compared to the Fenton process.

3.3 Reusability and stability of $CuFe_2O_4$

The reusability and stability of a catalyst are essential for practical application. For this purpose, the recycling efficiency of $CuFe_2O_4$ for the removal of CIP was studied in five cycles consecutively. Based on the result presented in Fig. 3a, the percentage of CIP removal using $CuFe_2O_4$ dropped to 49% after the fifth cycle. Previously, Wang and co-workers also observed a decrease in the percentage of norfloxacin removal using $CuFe_2O_4$ as an activator of peroxymonosulfate, from 91.8 to 78.3% after four cycles [41]. They attributed such a decrease in the percentage of removal to the conglomeration of the catalyst and occupation of the active sites of $CuFe_2O_4$ by norfloxacin or its intermediates [41]. However, the FTIR spectra of $CuFe_2O_4$ catalyst before use and after the fifth cycle presented in Fig. 3b did not show any significant change in the functional groups, indicating that the $CuFe_2O_4$ behaves as a catalyst and is structurally stable.

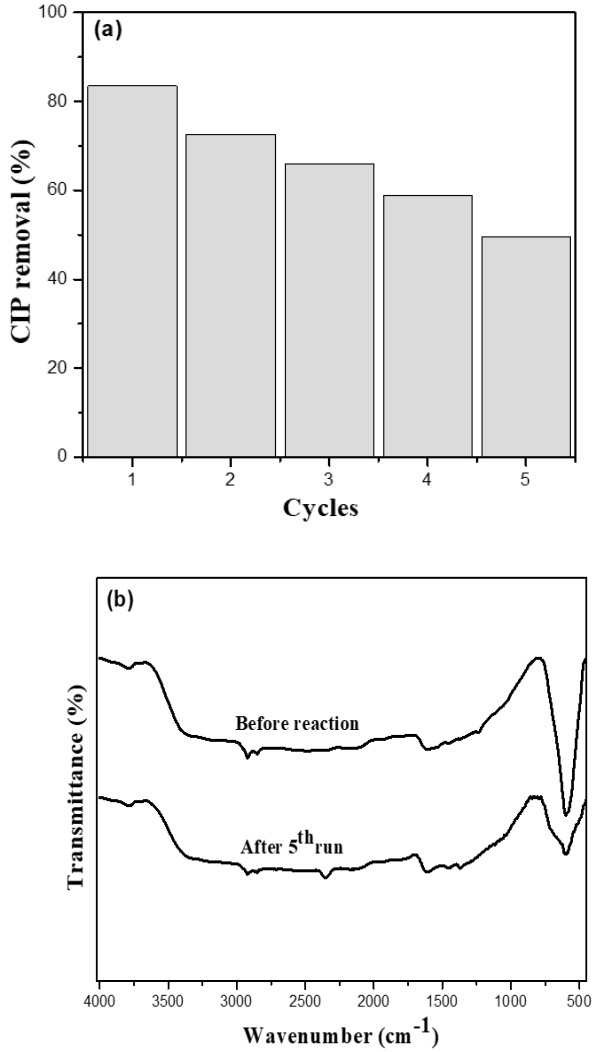

Fig. 3. (a) Reusability of $CuFe_2O_4$ catalyst in the removal of CIP from aqueous solution via Fenton reaction (b) FTIR spectra of fresh and used $CuFe_2O_4$ catalyst after the fifth cycle.

4. CONCLUSION

In the current study, $CuFe_2O_4$ catalyst was successfully synthesized via facile co-precipitation process and

characterized using various techniques. Subsequently, $CuFe_2O_4$ catalyst was used as an activator of H_2O_2 for the degradation of CIP from an aqueous solution. The degradation process was affected by several parameters such as catalyst dosage, the volume of H_2O_2, initial CIP concentration, inorganic ions, and solar irradiation. The optimal conditions for the removal of CIP from an aqueous solution using the $CuFe_2O_4$ catalyst are 1.0 g/L catalyst dosage, 0.5 mL of H_2O_2 and 2 h exposure under sun light. The highest removal percentage of more than 90% was recorded via the heterogeneous photo-Fenton degradation process under solar irradiation. The reusability study shows that the catalyst maintained reasonable efficiency, although a slight reduction was observed after the fifth cycle although the FTIR analysis revealed no changes in the surface functional group. Although further study should be done to improve the reusability of the $CuFe_2O_4$ catalyst, the current study revealed that it could be a good candidate for the treatment of wastewater contaminated by organic pollutants.

ACKNOWLEDGEMENTS

The authors gratefully thank Universiti Sains Malaysia for the financial support provided under RUI Grant No. 1001/PKIMIA/8011117.

REFERENCES

[1] X. Hou, J. Liu, W. Guo, S. Li, Y. Guo, Y. Shi, C. Zhang, Catalysis Communications 121 (2019) 27-31.
[2] N. Lu, P. Wang, Y. Su, H. Yu, N. Liu, X. Quan, Chemosphere 215 (2019) 444-453.
[3] S.S. Imam, R. Adnan, N.H.M. Kaus, Journal of Alloys and Compounds (2020) 155990.
[4] M.A.M. Yusoff, S.S. Imam, I. Shah, R. Adnan, Materials Research Express 6(8) (2019) 0850g5.
[5] S.S. Imam, R. Adnan, N.H.M. Kaus, SN Applied Sciences 1(8) (2019) 845.
[6] M. Malakootian, A. Nasiri, A. Asadipour, E. Kargar, Process Safety and Environmental Protection 129 (2019) 138-151.
[7] S.S. Imam, R. Adnan, N.H.M. Kaus, Colloids and Surfaces A: Physicochemical and Engineering Aspects 585 (2020) 124069.
[8] Y. Huang, L.-c. Nengzi, X. Zhang, J. Gou, Y. Gao, G. Zhu, Q. Cheng, X. Cheng, Chemical Engineering Journal 388 (2020) 124274.
[9] Y. Xiang, Y. Huang, B. Xiao, X. Wu, G. Zhang, Applied Surface Science 513 (2020) 145820.
[10] J. da Silveira Salla, K. da Boit Martinello, G.L. Dotto, E. García-Díaz, H. Javed, P.J. Alvarez, E.L. Foletto, Colloids and Surfaces A: Physicochemical and Engineering Aspects (2020) 124679.
[11] Y. Pang, H. Lei, Chemical Engineering Journal 287 (2016) 585-592.
[12] J. Wu, X. Wang, H. Kang, J. Zhang, C. Yang, International journal of environmental studies 71(4) (2014) 534-545.
[13] Z. Chen, L. Wang, H. Xu, Q. Wen, Chemical Engineering Journal 389 (2020) 124345.
[14] K. Faungnawakij, N. Shimoda, T. Fukunaga, R. Kikuchi, K. Eguchi, Applied Catalysis B: Environmental 92(3-4) (2009) 341-350.
[15] W. Shangguan, Y. Teraoka, S. Kagawa, Applied Catalysis B: Environmental 16(2) (1998) 149-154.
[16] M. Estrella, L. Barrio, G. Zhou, X. Wang, Q. Wang, W. Wen, J.C. Hanson, A.I. Frenkel, J.A. Rodriguez, The Journal of Physical Chemistry C 113(32) (2009) 14411-14417.
[17] D. Karimipourfard, R. Eslamloueyan, N. Mehranbod, Journal of Environmental Chemical Engineering 8(2) (2020) 103426.
[18] E.Z. Hegazy, I.H. Abd El-Maksod, A.M. Ibrahim, S.E.-S. El-Shafay, Bulletin of the National Research Centre 42(1) (2018) 9.
[19] X. Wu, F. Xia, Z. Nan, Materials Chemistry and Physics 242 (2020) 122490.
[20] R. Dhanda, M. Kidwai, RSC advances 6(58) (2016) 53430-53437.
[21] A.M. Naglah, M.A. Al-Omar, A.A. Almehizia, H.M. AlKahtani, A.J. Obaidullah, M.A. Bhat, N.S. Al-Shakliah, Journal of Inorganic and Organometallic Polymers and Materials 31(5) (2021) 2105-2115.
[22] K.C. Das, S.S. Dhar, Journal of Alloys and Compounds (2020) 154462.
[23] F. Foroughi, S. Hassanzadeh-Tabrizi, A. Bigham, Materials Science and Engineering: C 68 (2016) 774-779.
[24] G. Mathubala, A. Manikandan, S.A. Antony, P. Ramar, Journal of Molecular Structure 1113 (2016) 79-87.
[25] S.T. Fardood, F. Moradnia, M. Mostafaei, Z. Afshari, V. Faramarzi, S. Ganjkhanlu, Nanochem. Res. 4 (2019) 86-93.
[26] U. Naresh, R.J. Kumar, T.R. Parasad, Bulletin of Pure & Applied Sciences-Physics 37(2) (2018) 172-177.
[27] T.M. Hammad, J.K. Salem, A.A. Amsha, N.K. Hejazy, Journal of Alloys and Compounds 741 (2018) 123-130.
[28] E. Barsotti, S.P. Tan, M. Piri, J.-H. Chen, Fuel 263 (2020) 116441.
[29] S.S. Imam, R. Adnan, N.H.M. Kaus, Research on Chemical Intermediates 44(9) (2018) 5357-5376.
[30] I. Shah, R. Adnan, W.S.W. Ngah, N. Mohamed, PloS one 10(4) (2015) e0122603.
[31] E.M. Cuerda-Correa, M.F. Alexandre-Franco, C. Fernández-González, Water 12(1) (2020) 102.
[32] M.E. Ali, T.A. Gad-Allah, M.I. Badawy, Applied Water Science 3(1) (2013) 263-270.
[33] M.Y. Ghaly, G. Härtel, R. Mayer, R. Haseneder, waste management 21(1) (2001) 41-47.
[34] N. Azmi, O. Ayodele, V. Vadivelu, M. Asif, B. Hameed, Journal of the Taiwan Institute of Chemical Engineers 45(4) (2014) 1459-1467.
[35] Y. Deng, R. Zhao, Current Pollution Reports 1(3) (2015) 167-176.
[36] C. Bouasla, F. Ismail, M.E.-H. Samar, International Journal of Industrial Chemistry 3(1) (2012) 15.
[37] N. Singh, C. Balomajumder, Journal of water process engineering 9 (2016) 233-245.
[38] H. Hassan, B. Hameed, Chemical Engineering Journal 171(3) (2011) 912-918.
[39] J. Fick, H. Söderström, R.H. Lindberg, C. Phan, M. Tysklind, D.J. Larsson, Environmental Toxicology and Chemistry 28(12) (2009) 2522-2527.
[40] Y. Kanigaridou, A. Petala, Z. Frontistis, M. Antonopoulou, M. Solakidou, I. Konstantinou, Y. Deligiannakis, D. Mantzavinos, D.I. Kondarides, Chemical Engineering Journal 318 (2017) 39-49.
[41] Y. Wang, D. Tian, W. Chu, M. Li, X. Lu, Separation and Purification Technology 212 (2019) 536-544.